

TM: Symons. AS.

Code mrt

BELLCOMM, INC.

COVER SHEET FOR TECHNICAL MEMORANDUM

TITLE- A General Description of Radiative  
Heating for Re-entry at Lunar  
Return Velocities

TM- 64-1114-1

FILING CASE NO(S)- 110

DATE- May 22, 1964

AUTHOR(S)- H. L. Davis

FILING SUBJECT(S)- Re-entry  
(ASSIGNED BY AUTHOR(S)) Radiative Heating

*DRA*

ABSTRACT

This report is concerned with the highlights of and the uncertainties connected with calculating the radiative heating experienced by the face of a vehicle re-entering the earth's atmosphere at lunar return velocities. A description of the physical processes occurring as the air moves through and away from the shock front of a re-entry vehicle is first presented. Such a description leads to a natural splitting of radiative heating into two components, equilibrium and non-equilibrium radiative heating. Separate considerations of these two components leads to the following major conclusions: (1) Present equilibrium radiative heating calculations are uncertain by at least a factor of three. This uncertainty is mainly due to incomplete knowledge of the radiative intensity of hot air as a function of its temperature and density. (2) Present predictions of nonequilibrium radiative heating are uncertain by about a factor of two due to lack of precise experimental data. However, it is shown that the level of nonequilibrium radiation is so small compared to the total heating expected to be experienced by the Apollo CM, that this uncertainty will not affect the CM heat shield design. (3) To obtain any major improvement of the uncertainty present in radiative heating calculations, future work should concentrate on obtaining improved radiative intensity tables for high temperature air.

This report should be considered as preliminary and serving as background for future work which will more explicitly deal with the re-entry of the Apollo CM.

FACILITY FORM 602

N71	(THRU)
(ACCESSION NUMBER) 422683	NONE
(PAGES) OR - 117876	(CODE)
(NASA CR OR TMX OR AD NUMBER)	(CATEGORY)

SEE REVERSE SIDE FOR DISTRIBUTION LIST



DISTRIBUTION

COMPLETE MEMORANDUM TO

COVER SHEET ONLY TO

CORRESPONDENCE FILES:

OFFICIAL FILE COPY

plus one white copy for each  
additional case referenced

TECHNICAL LIBRARY (4)

J. A. Hornbeck  
B. Kaskey  
H. S. London  
C. A. Lovell  
C. R. Moster  
J. E. Parker  
I. M. Ross  
J. A. Saxton  
R. R. Schreib  
R. W. Sears  
T. H. Thompson  
J. M. West

Division 111

Division 212

All Members, Division 111

# BELLCOMM, INC.

---

SUBJECT: A General Description of  
Radiative Heating for Re-entry  
at Lunar Return Velocities -  
Case 110

DATE: May 22, 1964

FROM: H. L. Davis

TM-64-1114-1

## TECHNICAL MEMORANDUM

### I. INTRODUCTION

This report is concerned with a description of the radiative heating experienced by vehicles entering the Earth's atmosphere at lunar return velocities. To this end, we will first give a simplified description of the physical processes involved. Such a description will enable us to split the radiative heating into two components, equilibrium and non-equilibrium, each of which will then be discussed at length. Our discussions will be kept as general and simple as possible with the aim being to explain as many of the highlights and difficulties of calculating radiative heating without introducing unnecessary detail. This background will thus set the stage for future work explicitly dealing with re-entry of the Apollo CM where more detail and a critical analysis of the uncertainties will be presented.

In calculating the radiative heating experienced by a re-entry vehicle, knowledge of the local temperature in the flow field about the vehicle is required. Detailed information of the temperature and density distribution in the flow field enables an integration to be performed which gives the radiative heating flux input at a given point on the re-entry vehicle. That is, each elemental volume in the flow field may be thought of as a radiating body with an effective emissive power which is obtainable from tables if the temperature and density of the elemental volume are known. The radiative heating rate at a given point on the vehicle is then obtainable by integrating over the elemental volumes in the flow field which are seen by the given point. A detailed description of this process, including the emissive power tables, will be reserved until a later section. In this section only a simplified description of the physical processes involved in radiative heating will be given.

The important physics in radiative heating is a knowledge of how the temperature changes as the air moves through the flow field. This change in temperature is schematically shown in Figure 1. Region A of the figure represents the air flow in front of the re-entry shock where the air is moving, relative to the vehicle, with a velocity  $U_\infty$ , and has the ambient temperature and density of  $T_\infty$  and  $\rho_\infty$ . Since the thermal energy corresponding to a  $T_\infty$  of a few hundred °K is small relative to

the kinetic energy at lunar return, the total energy of the air is approximately equal to its kinetic energy. For an initial re-entry speed of 36,000 ft/sec, this kinetic energy is 26,000 BTU per lb. of air, or about 18 ev per molecule. As the air passes through the shock front, almost all of this kinetic energy is transferred to internal and thermal energy, since the flow speed goes subsonic as air moves through the shock front of a blunt re-entry vehicle. In absorbing this kinetic energy, all possible thermal modes of the air molecules are used. However, not all the modes have the same excitation times. Usually the translational-rotational modes are the first to absorb the energy, with the vibrational-dissociational-ionizational-electronic modes lagging behind. The specific lag time for these latter modes depends on collision rates, which in turn have a density dependence. This means as the air moves through the shock front, practically all the free-stream kinetic energy is initially transferred into translational-rotational thermal motions of the air molecules. Of course, the work done in compressing the gas in moving through the shock must be subtracted from the initial kinetic energy.

Although the air is not in thermal equilibrium in region B, it is convenient to refer to a temperature for the air. Our reference temperature in this region will be the temperature corresponding to the translational thermal motions. Thus, using the arguments of the preceding paragraph, in that part of region B just behind the shock front, the translational temperature may be obtained by considering air to be a perfect diatomic gas. When this is done, the translational temperature,  $T_i$ , just behind the shock front is given by the Rankine-Hugoniot relationships for  $\gamma = 7/5$  ( $\gamma$  = ratio of specific heats = 7/5 for a perfect diatomic gas). For a flight Mach number  $M$ , these give

$$T_i/T_\infty = (35 - 5/M^2) (1 + 0.2M^2)/36, \quad (1 - 1)$$

which has been derived on the assumption of a perfect diatomic gas with compression of the gas through the shock front being taken into account. Eq. (1 - 1) gives a  $T_i$  in the range 40,000 - 75,000 °K for velocities in the range 30,000 - 40,000 ft/sec.

As the air moves into region B of Figure 1, some of the energy stored in the translational-rotational modes is gradually transferred to other modes via collisions between the air molecules. The transfer rate depends upon the collision rate for the pertinent type of transfer. This energy transfer causes the translational temperature to drop as shown in the temperature diagram of Figure 1. The drop then continues until true thermal equilibrium is achieved. To obtain the final equilibrium temperature, it is necessary to use thermodynamic tables <sup>2-5</sup> for air which have been calculated by taking into account all mechanisms

which can absorb energy; e.g., translation, rotation, vibration, dissociation, ionization, electronic excitation, interactions between particles, etc. Using these tables, the initial kinetic energy of 26,000 BTU/lb gives an equilibrium temperature for hot air in the 9,000 - 12,000 °K range depending upon the vehicle altitude. The region C of Figure 1 corresponds to that part of the flow field where thermal equilibrium has been achieved.

Knowing the temperature variation in the flow field allows the radiative intensity of each part of the flow field to be discussed. A visual description of the radiative intensity throughout the flow field is given in the lower diagram of Figure 1. Although the rise in translational temperature may be thought of as being instantaneous as the air passes through the shock front, the hot air does not immediately possess a radiative intensity corresponding to the translational temperature. Generally, this is due to the finite time required for the mechanisms which populate the excited states furnishing the radiation. Specifically, complete detailed theoretical understanding of this rise time is not available; however, shock-tube experiments and qualitative theories give verification to the general shape illustrated in Figure 1. Thus, as the air passes through the shock front, the radiative intensity starts to rise from essentially zero and continues to rise as the air moves away from the shock front until a maximum is achieved. Occurrence and location of the maximum in the radiative intensity is determined by the counteraction of the decrease in translational temperature. After reaching its maximum value, the radiative intensity decreases, following the temperature decrease, until it reaches an equilibrium value corresponding to the equilibrium temperature.

It is seen from the above discussion that any description of radiative heating can be naturally split into two parts. One part which pertains to the nonequilibrium radiation (region B), and the other which pertains to equilibrium radiation (region C). Each of these will be treated at length in later sections of this report. Before so proceeding, it is important to note that Figure 1 is only meant to be a schematic representation of the radiation profile in front of a re-entry vehicle. The point to be made is that the relative sizes of regions B and C can vary considerably depending upon  $U_\infty$  and  $p_\infty$ . In fact, region B can vary from a very thin layer just behind the shock front (usually at lower altitudes) to filling the entire flow field about the re-entry vehicle (usually at higher altitudes). Explicit examples of this variation will arise in the remainder of this report.

## II. EQUILIBRIUM RADIATION

To calculate the radiative heating experienced by a re-entry vehicle due to the equilibrium hot air (region C of Figure 1) in front of the vehicle, details concerning the flow field about the vehicle are required. These details are the temperature-density distributions for the hot air surrounding the vehicle. This input is to be obtained from flow field calculations and is hereafter assumed known for the purposes of this report. The equilibrium region can then be divided into volume elements and the radiative heating flux at any arbitrary point on the vehicle can be calculated by integration. Such a calculation would be rigorous if no absorption of the radiation occurred and/or no radiative decay (cooling) occurred in air. Radiative decay is a lowering of the temperature of the air due to energy (radiation) being lost by the air with a resultant drop in the radiative intensity of the air. Neglecting both of these effects would give over estimates for the radiative heating of a re-entry vehicle; however, these effects are relatively minor at lunar return velocities so the over estimation is expected to be slight. Hence, it is felt justified to first neglect these minor effects in our discussion in order to bring out the more dominant and straightforward aspects of radiative heating. Then the absorption and decay aspects will be discussed as a perturbation on the dominant ones.

A qualitative review of equilibrium radiative heating has been given by Wick<sup>6</sup> and our discussion in this section will somewhat parallel his, with our contributions being quantitative amplifications and specific direction to Apollo. Using the assumption of thermal equilibrium (i.e., region C of Figure 1 is assumed to fill the entire region between the shock front and the vehicle), an idealized case of stagnation point radiative heating is first discussed. Then, using this case as a reference point, more realistic cases will be treated as the section progresses. It is to be noted that many generalities will be made in our discussion with the purpose being to stress, one by one, some of the more important aspects of the problem of equilibrium radiative heating. Furthermore, the approach in this section will mainly be one- or two-dimensional, since the purposes of this report can be served without the added difficulty of considering the three-dimensional case.

Stagnation Point Heating -- Plane-Layer Approximation

As our first example, consider the geometry of a plane vehicular wall with a plane shock front detached a distance  $\delta$  from the wall as illustrated in Figure 2. Schematically shown in the figure is an elemental volume of hot air radiating in all directions. This plane-layer approximation has the beauty of simplicity and the merit of accuracy for many practical cases. There are two reasons for this: (1). The actual shock layer approaches a plane layer in some practical cases because  $\delta$  is small compared to the vehicular radius of curvature. (2). The temperature and density of the air do not differ significantly in those portions of the shock layer which contribute most of the radiation to the stagnation point. Under the assumptions of uniform temperature behind the shock front and no reflection or emission by the wall, the radiative flux,  $q_s$ , at point S on the wall of Figure 2 is

$$q_s = \frac{E_T}{2} \int_0^{\pi/2} \sin \theta \, d\theta \int_0^{\delta} x \, dx$$

$$= \frac{E_T}{2} \delta \quad (2-1)$$

The quantity  $E_T$  is the radiative energy flux from a unit volume with the factor  $1/2$  to account for the fact that half the radiation is directed away from the wall. As is seen, the radiative flux at S is completely determined if  $E_T$  and  $\delta$  are known.

 $E_T$  Tables

To determine  $E_T$  extensive theoretical and experimental work has been done by the Avco group (explicit references to this work may be found in reference 7). Using this work Kivel and Bailey<sup>7</sup> have published  $E_T$  for air in tabular form as a function of density and temperature. Furthermore, such data can be plotted<sup>8</sup> in the simple graphical form of Figure 3. The density-temperature region where Avco shock tube measurements have approximately verified the  $E_T$  values is indicated by the

dotted area on Figure 3. Data corresponding to Figure 3 is sometimes stated as the emissivity per unit length  $\epsilon$ . Then the same radiative flux given by Eq. (2 - 1) would be

$$\dot{q}_s = \epsilon \delta \sigma T^4, \quad (2 - 2)$$

where  $\sigma$  is the Stefan-Boltzman constant and the correspondence  $E_T = 2\epsilon\sigma T^4$  is made. When this is done the data of Figure 3 can be represented<sup>9</sup> by the correlation formula

$$\epsilon \approx .50 \left( \frac{\rho_s}{\rho_o} \right)^{1.30} \left( \frac{T_s}{10^4 \text{ } ^\circ\text{K}} \right)^{8.5} \text{ cm}^{-1}. \quad (2 - 3)$$

Here  $\rho_o$  is ground atmospheric density,  $\rho_s$  is the density of the air behind the shock front, and  $T_s$  is the temperature of the air behind the shock front. Expression (2 - 3) reasonably approximates Kivel and Bailey's tables in the region  $8000 \text{ } ^\circ\text{K} \leq T_s \leq 12,000 \text{ } ^\circ\text{K}$  and  $10^{-4} \leq \rho_s/\rho_o \leq 10^{-2}$ . As an independent check on Kivel and Bailey's tables, we refer to calculations to determine  $E_T$  performed by Meyerott et. al.<sup>10</sup>. The results of these calculations have been plotted by Thomas<sup>11</sup> in the form of Figure 4. Thomas has also given an approximate correlation to these calculations of

$$\epsilon \approx 0.138 \left( \frac{\rho_s}{\rho_o} \right)^{1.28} \left( \frac{T_s}{10^4 \text{ } ^\circ\text{K}} \right)^{6.54} \text{ cm}^{-1} \quad (2 - 4)$$

for the region  $8,000 \text{ } ^\circ\text{K} \leq T_s \leq 16,000 \text{ } ^\circ\text{K}$ . The Kivel and Bailey results are consistently higher than the calculations of Meyerott et. al. Kivel<sup>12</sup> has discussed the uncertainty in Kivel and Bailey's values and noted that they could be high by a factor of 2. Other  $E_T$  calculated values have been presented by Breene et. al.<sup>13</sup> which lie between the results of Meyerott et. al. and those of Kivel and Bailey for temperatures and densities of interest during lunar return.

Even the most recent experimental results have been unable to completely distinguish which of the  $E_T$  values is more correct. For example, Page of Ames<sup>14</sup> has measured the radiation from the shock layer about small gun-launched models flying in still air or upstream through the shock produced by a hypersonic wind tunnel. In this manner, he was able to simulate vehicle velocities up to 41,000 ft/sec. Although his results tended to favor the higher predictions of the AVCO and GE groups, there



was enough experimental scatter to make it difficult to really choose between any of the three  $E_T$  predictions. This scatter can be seen in Figure 5 which is a plot of the total measured radiation flux vs. simulated velocity. The radiation intensity is presented with the normalizing factor  $(\rho/\rho_0)^{1.7}$ , since both the experiments and equilibrium radiation predictions shown indicate that the intensity should vary as this power of the density at constant velocity. Undoubtedly some of this scatter is due to different model materials used to obtain the data, since the plastic models were known to be ablating and tests have shown that ablation products can increase the radiation level. However, even with this taken into account, it is seen from Figure 5 that these results do not uniquely distinguish which set of  $E_T$  values is more correct. Also clouding the picture for  $E_T$  tables, is a recent GE<sup>15</sup> report, dealing with radiation with wavelengths less than  $.2\mu$ , which theoretically predicts considerably more radiation in this region than previous investigations. This is important because most laboratory experiments can only crudely measure radiation in this wavelength region due to, for example, quartz windows used to isolate radiometers which are opaque to this radiation. Using these new GE tables in the usual manner by assuming the hot air is optically thin (no absorption) leads to an approximate doubling of the expected radiative heating on the Apollo CM over that calculated using the Kivel and Bailey tables. The need for more theoretical and experimental investigation in this area is evident. In summary, the present uncertainties in  $E_T$  tables are such that the author believes one cannot predict radiative heating loads for lunar return to better than a factor of 2 or 3. This may be easily seen by considering the experimental scatter shown on Figure 5 for the velocity range 28 to 36 kft/sec.

#### Stagnation Point Heating -- Spherical Segment Shock

A more realistic model than the plane shock is a spherical segment wall surrounded by a spherical segment shock front as illustrated in Figure 6. The portion of the hot air which will radiate to point S is shaded on the figure. Under the same assumptions used in the plane model, the radiative flux at S is

$$\dot{q}_S = (E_T/2) \delta \int_0^{\pi/2} d\theta \sin\theta \int_0^{x_\theta/\delta} dx$$

$$= (E_T/2) \delta K_S$$

(2 - 5)

It is seen that the flux for this model differs from the flux for the plane model by a factor  $K_s$ , which we will call a "shock shape factor," and due to the point S seeing a different volume of hot air here than in the plane-layer case. Comparing the results for the plane and spherical segment, it is seen that in addition to  $E_T$ , one must have a knowledge of the shock detachment distance and the shock shape factor to predict the radiative heating flux experienced during re-entry. These latter quantities will now be considered.

#### Shock Detachment Distance

An illustration of the variance of the shock detachment distance with vehicular shape is shown in Figure 7. In the figure, the detachment distance is given as a function of the ratio  $\rho_\infty/\rho_s$  and the ratio  $R/D$ . By way of explanation, a vehicle with  $R/D = 0.5$  is a hemisphere, while the Apollo CM approximates a vehicle with an  $R/D$  of about 1.2. Figure 7 was calculated by Wick<sup>6</sup> using a method developed by Kaattari.<sup>16</sup> This method for predicting  $\delta$  is based on oblique and normal-shock relationships and the continuity of mass flow through suitably chosen volume elements between the shock and vehicle. Furthermore, Kaattari's predictions have been shown to be in good agreement with experimental results for both perfect and real-air cases up to about Mach 20 by using small scale models in hypersonic wind tunnels. But there is no experimental confirmation for lunar return speed or for vehicles of the larger Apollo CM size. However, as noted on Figure 7, the shock detachment distance is primarily determined by the density ratio through the shock front which is obtained by reference to calculated thermodynamic tables based on normal-shock relationships (e.g., see reference 2). Thus, if these tables can be trusted, Figure 7 should be relatively accurate, compared to the uncertainties in  $E_T$ , for the lunar return case, but these tables have not been completely checked with experimental results. To be certain, one would like experimental verification of Figure 7 for lunar return velocities. Noted on Figure 7 is the range of density ratios for the broad range of flight velocities and altitudes indicated on the figure, showing a good value of  $\delta/R$  for quick calculations of radiative heating is 0.045.

#### Shock Detachment Distance -- Non-Zero Angle of Attack

The effect of non-zero angle of attack on the shock detachment distance has also been considered by Wick. His results for spherical segment vehicles are given in Figure 8 in the form of the ratio of the stagnation standoff distance

at angle of attack to the corresponding value at zero angle of attack. Again, the results of Figure 8 were calculated by Wick using Kaattari's method, which again has been shown<sup>17</sup> to give good agreement with experimental results with the same limitations to Apollo as discussed for the zero angle of attack case. All the curves of Figure 8 terminate at the dotted line designated as the limit of the theory which is defined by the angle of attack at which the free stream velocity becomes parallel to the straight edge of the spherical segment vehicle. The most interesting result illustrated in Figure 8 is that the detachment ratio has a value of about 0.43 for the limiting case for the theory. This means that for radiative heating the spherical segment vehicle has an effective nose radius of 0.43 times the geometric radius for the limiting case.

#### Shock Shape Factor

Calculation of the shock shape factor is only a problem of numerical integration once the shock detachment distance is known. Wick's results for the shock shape factor are given in Figure 9. He found, for the range of spherical segment vehicles shown on the figure, that this factor is only a function of density ratio across the shock front. From the figure it is seen that the shape factor does not differ much from unity; thus, in view of the uncertainties in  $E_T$ , use of a value of 1.0 would be justified. However, if completeness is desired, a value of 0.84 is a good average value to use in the velocity-altitude range of interest for lunar return.

#### Summary of Stagnation Point Radiative Heating

It is to be remembered that the above comments have been for the case of stagnation point radiative heating only, while a discussion of the distribution over the vehicle is yet to be described. With the information given in Figures 2 through 9, rapid estimates of equilibrium radiative flux for the stagnation point can be made for a variety of vehicle shapes and wide ranges of velocity and altitude. Probably the most serious limitation to accurate stagnation point calculations is the inability to obtain accurate  $E_T$  values. As previously discussed, present uncertainties in  $E_T$  limit calculation of the radiative heating load for lunar return to no better than a factor of 2 or 3 from a reference value defined by Kivel and Bailey's tables. Although no direct experimental results have verified the calculated shock detachment distance, it is the author's belief that this uncertainty is not so serious as the

ones connected with the values of  $E_T$ . Thus, in summary, since the stagnation point radiative flux has a direct proportionality to both  $E_T$  and  $\delta$ , one is unable to further specify  $q_s$  beyond saying it is probably within the boundaries defined by values which are up or down by a factor of 3 from the value which would be obtained by using Kivel and Bailey's  $E_T$  values and Kaattari's method to obtain  $\delta$ . Before proceeding, it is worthwhile to note that application of the above concepts leads to maximum radiative heating rates of the order of 1000 watts/cm<sup>2</sup> on the Apollo CM for the HES-6 trajectory (escape speed entry).

### Radiative Heat Flux Distributions

In order to calculate radiative heat flux distributions over re-entry vehicles, a detailed analysis of the temperature and density distributions in the flow field about the vehicle must be available. As mentioned before, this report assumes such are available and no detailed description will be given concerning calculation of these quantities. Once they are available,  $E_T$  can be obtained from tables for each elemental volume in the flow field. The final step is then a lengthy integration of the radiation from all the elemental volumes in the flow field. However, if only approximate answers are desired, it is possible to use a plane-layer approximation pointed out by de l'Estoile and Rosenthal.<sup>18</sup> In this manner the necessary labor is considerably reduced without introducing significant errors (say, no more than 20%). This method has considerable merit when one considers the large uncertainty in  $E_T$ . An example of this method is shown in Figure 10 which illustrates its application to a point X away from the stagnation point S. The radiative flux at X is then approximated by the simple integral.

$$q_x = \int_0^{\delta} [E_T(y)/2] dy \quad (2 - 6)$$

The complete plane layer approximation is then replacing the integral by a sum over a finite (usually small) number of plane layers; i.e.,

$$q_x = \sum_{i=1}^n [E_T(i)/2] \delta_x(i) \quad (2 - 7)$$

with  $E_T(i)$  corresponding to the mean temperature in the i-th plane and  $\delta_x(i)$  the thickness of the i-th plane. Of course, the accuracy of the method depends upon the number of layers used in the analysis. Also, in application of the method, one could apply shock shape factors for each layer. But this would detract from the basic simplicity of the method and require about the

same amount of work as integration over the volume seen by the point X. However, in the method it is necessary to consider more than one plane layer because of temperature-density variations between the shock front and the vehicular wall.

An illustration of typical temperature-density variations has been given by Wick and is shown on the right of Figure 10. Also shown is how these variations cause  $E_T$  to vary between the shock front and the wall. The most interesting feature of the variations is how relatively minor temperature-density variations can cause a large variation in the radiative intensity of the gas. It is seen from the figure that a temperature just 97% of the stagnation temperature gives a radiative intensity for the air just in front of point X of about 65% of the radiative intensity just in front of point S. This strong variation is primarily due to the small change in temperature, since the radiative intensity goes approximately as the eleventh power of the temperature [e.g., see Eqs. (2 - 2), (2 - 3), and (2 - 4)] while it has only small dependence on the density. This example excellently illustrates the necessity of having accurate temperature distributions within the flow field; e.g., a 5% error in temperature can cause a 70% error in radiative intensity, while a 10% error in temperature would cause a 180% error in radiative intensity. Temperatures in the flow field are obtained by knowing the local velocities and densities, and the free stream velocity and density; then by equating enthalpies the local temperature can be obtained from thermodynamic tables for air. The point is that these tables are primarily based on detailed calculations which to the author's knowledge, have had no direct experimental checks on their accuracy in the temperature range of interest for lunar return.

Wick has obtained radiative distributions over the blunt face of spherical segment re-entry vehicles. His calculations were based on temperature-density distributions just behind the shock front obtained by using normal-shock properties given by Hochstim<sup>19</sup> and then using oblique-shock theory. To obtain the same distribution at the vehicular wall, he used work by Kaattari<sup>20</sup>; for points between the shock front and face he made a linear interpolation. Wick justified this simplified procedure by comparison of its results with more detailed calculations made by Maslen and Moeckel<sup>21</sup> for blunt body shock layers and real air conditions; and by Fuller<sup>22</sup> for hemispherical shocks and perfect gases.

Some radiative distribution results of Wick for zero angle of attack are given in Figure 11 which is a plot of the ratio of local wall radiative flux to stagnation flux as a function of face position and the ratio  $R/D$ . The lines on the figure are for the mean of the velocity-altitude range

shown on the figure, with slight deviations from the lines occurring over the range of velocity-altitude shown on the figure. It is seen from Figure 11, as could be expected from any considerations of the effect of the R/D ratio on temperature-density variations, the less the value for R/D, the more rapid is the decrease in wall radiative flux moving away from the stagnation point.

Some of Wick's results on the variation of the radiative flux distribution with angle of attack are given in Figure 12. These results are, as shown on the figure, for angles of attack of  $0^\circ$ ,  $-15^\circ$ , and  $-30^\circ$  with the flux distribution being normalized with respect to the stagnation value at zero angle of attack. In this way the curves can show not only the change in flux distribution but also the change in stagnation level at the various angles of attack. The tick marks on the curves are the locations of the stagnation points, with the velocity-altitude applicability being the same as Figure 11. The fact that the location of peak flux is not always the stagnation point is due to the opposing effects of increasing shock detachment distance and decreasing temperature as one goes away from the stagnation region. In Figure 12, as in Figure 11, the lines are for the mean of the velocity-altitude range considered, with slight deviations occurring over the range of these quantities.

From the above paragraphs it is seen that the flux distribution should be subject to about the same uncertainties as those discussed for the shock detachment distance at zero angle of attack. There will be also uncertainties entering into the flux distributions due to inaccuracies of the temperature-density distributions in the flow field. Since this is essentially a flow field problem, it will not be discussed here. But any uncertainties present in flow-field calculations affecting the temperature-density distributions would cause  $\dot{q}_x$  to be more uncertain than  $\dot{q}_s$ , which itself is uncertain within a factor of 3.

#### Effect of Decay and Absorption

To account accurately for the effects of decay and absorption on the radiative heating experienced by a re-entry vehicle, the basic radiative transfer equations would have to be coupled with the appropriate hydrodynamic equations for the flow field. In doing this, one would find rather formidable integro-differential equations to solve. The solutions of these equations are so complex that no solutions for three-dimensional shocks are present in the existing literature. In fact, to say anything about these effects one must refer to some one- and two-dimensional results which are in the existing literature. 6,23-27 Since this is an extremely detailed subject,

we will only state in this report the results of the one-dimensional investigations. The results are best stated in terms of characteristic lengths for decay,  $L_{dec}$ , and for absorption,  $L_{abs}$ . These characteristic lengths are defined by

$$L_{dec} = \frac{(1/2)\rho_{\infty}V_{\infty}^3}{E_T} \quad , \quad (2 - 8)$$

and

$$L_{abs} = \frac{1}{\epsilon(T)} \quad (2 - 9)$$

The magnitude of the detachment distance  $\delta$  compared to these characteristic lengths then determines when the effects become important. Important being defined as when the effects change the radiative flux at the vehicle more than, say, about 5%. The results of the one-dimensional investigations are, roughly, that decay becomes important when

$$\delta \geq 0.1 L_{dec} \quad , \quad (2 - 10)$$

and absorption becomes important when

$$\delta \geq 0.1 L_{abs} \quad . \quad (2 - 11)$$

Upon detailed examination it is found that the above conditions are not met within the re-entry corridor for the Apollo CM where any significant amount of radiative heating occurs. Thus we were justified in neglecting these effects in our discussion until now. An exception to this statement could be any radiation with wavelengths below  $.2\mu$ . If the GE predictions<sup>15</sup> are correct in this region, the emissivity of the gas would be approaching the black body limit in this region and the specific wavelength analogue of Eq. (2 - 11) would be met in part of the  $< .2\mu$  region. A detailed discussion of this "Breene radiation" will be presented in a future report and further comments on this problem will be reserved for inclusion therein. In any event, neglect of absorption and decay will always cause an over estimation of radiative flux. The amount of over estimation depending upon  $L_{dec}$  and  $L_{abs}$ . An interesting fact, but not applicable to lunar return, is that large decay effects could also affect the convective heating flux due to the outer edge of the boundarylayer at the wall being cooler because of radiative decay. The process of radiative cooling reducing air ionization and then convective flux has been discussed by Adams.<sup>28</sup>

Summary of Equilibrium Radiative Flux

The above discussion of equilibrium radiative heating has purposely been limited to one- and two-dimensional cases in an effort to keep the discussion and illustrations as simple as possible. However, any uncertainties in these cases will carry over to the three-dimensional case, which itself contributes uncertainties due to the more difficult theoretical problem of predicting three-dimensional shock shapes and detachment. Since we have shown unquestionably that  $E_T$  uncertainties introduce errors of the order of two or three, that uncertainties exist in shock shape and detachment due to lack of good experimental data, and  $E_T$  has a very strong temperature dependence making accurate temperature distributions a necessity, the author believes a sound statement is that equilibrium radiative heating calculations for lunar return contain uncertainties of at least a factor of three.



### III. NONEQUILIBRIUM RADIATION

Since there is no clear boundary between regions B and C of Figure 1, an arbitrary definition of the nonequilibrium region is in order. We will follow the AVCO group and define the nonequilibrium region (Region B of Figure 1) as that portion of the flow field between the shock front and a boundary behind the shock front where the overshoot in the radiation intensity is 10% higher than the equilibrium value. A satisfactory theory describing all the properties of this region has yet to be developed. A complete theory would require detailed accounting of all the chemical and radiation processes occurring in the region, while a satisfactory theory would use only the dominant processes to obtain approximate answers. Lack of a quantitative theory is due to incomplete knowledge of the various chemical and radiation rate constants at the elevated translational temperatures occurring in the nonequilibrium region. Even if all the necessary rate constants were known, extremely detailed combinatorial work would have to be done to sort out the dominant reactions. Also, even knowing all the chemical reaction rates would still not enable radiation intensity calculations to be performed due to lack of knowledge concerning the radiative processes. That is, numerical descriptions are required of the collisions which excite the electronic levels whose de-excitation furnish most of the nonequilibrium radiation. Thus, the status of the theory for the nonequilibrium radiation may be stated as it is believed it is known what has to be done to obtain a theory but the required mass of experimental data (chemical and radiation rate constants) necessary to perform theoretical calculations is not yet available.

Experimentally, some shock tube studies have been performed which measure the nonequilibrium radiation as a function of shock velocity and tube density. Coupling these measurements with the incomplete theory has enabled reasonably accurate estimates to be made concerning the nonequilibrium radiative heating which would be experienced by a re-entry vehicle. Thus, this section will mostly be a description of the experimental measurements interspersed with exceedingly general theoretical comments. From this description, it will be seen that the level of the nonequilibrium radiative heating contribution compared to the total heating of the Apollo CM is so small that errors of even a factor of five in this component would not seriously affect Apollo heat shield design criteria considering the uncertainties in the equilibrium radiative flux and the magnitude of the convective heating.

To illustrate the radiative intensity behind a shock front, some typical oscillograms of radiative intensities are shown in Figure 13. These oscillograms were obtained at AVCO<sup>8</sup> by monitoring a cross-section of the shock tube as the shock moves pass this section by use of the apparatus illustrated in Figure 14.

The date of Figure 13 is for only the  $N_2$  First Negative Band (wavelength .55 to  $1.0\mu$ ) and obtained with an ambient gas of pure  $N_2$  at a pressure of 2 mm Hg. The results shown in Figure 13 verify, at least for these specific cases, the shape of the radiative intensity curve in Figure 1. Also immediately evident from Figure 13 is a steep dependence of the nonequilibrium peak on the shock velocity and a decrease of the width of the nonequilibrium region with velocity. Data similar to Figure 13 has also been obtained at AVCO with air being the ambient gas. Examples with air are given in Figures 15 and 16.<sup>8,29</sup>

Of course, the data of Figures 13, 15, and 16 is for only limited wavelength regions, while the solution of the radiative heating problem requires a complete spectra coverage at many velocities. Fortunately the AVCO group has undertaken such a study using air as the ambient gas by using a variety of measuring techniques. These studies allow the spectrum of the radiation originating in the nonequilibrium region to be synthesized. Examples of the results are given in Figures 17 and 18.<sup>8,30</sup> The total radiation from the nonequilibrium region can be obtained from Figures 17 and 18 by determining the area under the data points. This has been illustrated on Figure 18 with a dashed line drawn to give a generous envelope for the data points. The area under the dashed line is  $40 \text{ watts/cm}^2 - 2\pi \text{ steradians}$ , which is the intensity of nonequilibrium radiation being emitted by one side of an infinite slab or just the thickness of the nonequilibrium region at  $10 \text{ mm}/\mu \text{ sec}$  ( $32,800 \text{ ft/sec}$ ). This is a very conservative estimate since the AVCO group purposely drew the dashed line high where the least measurements were available and where large contributions could physically originate. It is also to be noticed that Figure 18 contains one data point for wavelengths below  $.2\mu$ . This point was obtained as a single measurement on the band between  $.075\mu$  and  $.14\mu$  by use of a tungsten photoelectric gauge. Although there are probably some minor uncertainties in this measurement due to gauge calibrations, this point does prevent the large uncertainties introduced for the equilibrium  $E_T$  values due to the less than  $.2\mu$  region being introduced for the nonequilibrium radiation. Certainly one would think that AVCO would have used the same techniques to obtain equilibrium radiation measurements in the less than  $.2\mu$  region. To date, the present author has been unable to find such data.

Some general theoretical comments are now in order concerning the nonequilibrium radiation profile. These comments will then be verified by reference to experimental data. In Figure 19, a schematic nonequilibrium radiation profile is given to illustrate the density independence of the total nonequilibrium radiation at a given velocity behind a normal shock. As the air moves through the shock layer, there is an excitation time for the radiative intensity to reach its maximum value,  $t_p$ , and a relaxation time for the radiative intensity to decay to 110% of the


equilibrium value,  $t_{1.1}$ . From these times the corresponding excitation,  $d_p$ , and relaxation,  $d_{1.1}$ , distances behind a normal shock are obtained by multiplying the times by the normal shock velocity  $U_\infty$ . These distances (times) are determined by collision rates for the air particles, since in the excitation or relaxation the energy transfer occurs via collisions. As long as the collision processes are binary (two particle collisions),  $t_p$  and  $t_{1.1}$  will approximately vary inversely as the first power of the density for constant velocity; i.e., the collision rate is directly proportional to the first power of the density at constant temperature.<sup>31</sup> Since the temperature dependence of the collision rate is as the inverse square root,<sup>31</sup> times  $t_p$  and  $t_{1.1}$  should approximately vary as stated if the magnitude of the translational temperature changes are about the same for difference densities at constant velocity. Then, under these conditions,  $d_p$  and  $d_{1.1}$  should vary as the inverse of the first power of the density. Also, under binary conditions, the peak radiative intensity,  $E_p$ , should vary directly with the number of radiating particles present, or directly with the density. A detailed argument verifying this statement using chemical and radiative rate equations may be found in reference 30. These binary collision arguments lead to the relations depicted on Figure 19; namely, (a)  $d_{1.1} \sim 1/\rho$  (b)  $E \sim \rho$  and (c) the total nonequilibrium radiation is independent of density. That is, the total nonequilibrium radiation mainly depends upon the shock velocity. In other words, as long as the nonequilibrium zone does not engulf the re-entry vehicle, the nonequilibrium radiative flux is primarily determined by the velocity and not the vehicle height (density).

The binary results described in the preceding paragraph have been reasonably well verified by AVCO and Ames experimental data. For example, Figure 16 shows some verification of this "binary scaling" for the total nonequilibrium radiation, since the areas under the two curves in this figure are constant to within 25%. Considerable other data exists which shows that the nonequilibrium region is reasonably well described by the simple binary collision model sketched here.<sup>8,14,29,30</sup> From an analysis of this data, I would say binary scaling is verified to within a factor of two for the velocity-density ranges of primary interest during lunar return except those regions where "truncation" occurs. Truncation will occur when the density is sufficiently small so that the relaxation distance  $d_{1.1}$  is larger than the shock detachment distance. That is, since  $d_{1.1}$  is inversely proportional to the density, at a high enough altitude, the entire shock layer will be filled with the nonequilibrium region. Thus, with increasing height, the nonequilibrium flux arriving at the vehicle will diminish

slowly from its full value when  $d_{1.1} > \delta$  but  $d_p < \delta$  and then more rapidly when  $d_p > \delta$ . It has been estimated <sup>32p</sup> that for lunar return the nonequilibrium radiation reaching the vehicle face starts to diminish at 250,000 ft. and will be less than its full value at higher altitudes because of truncation. But using existing measurements on the nonequilibrium radiation behind normal shocks, especially the measured values of  $t_p$  and  $t_{1.1}$ , even this insignificant (less than 1% of the total heating) radiative flux can be reasonably well estimated. It should be noted that the nonequilibrium zone extending to the vehicle can affect the convective heating, probably causing a slight increase, <sup>35</sup> since the transfer of heat across the boundary layer depends on the transport properties of hot air which are different for equilibrium and nonequilibrium hot air.

Below 250,000 ft the nonequilibrium radiative flux reaching the vehicle face depends only on the vehicle velocity. A total nonequilibrium flux vs. velocity summary of existing data from normal shock experiments is given in Figure 20 which is from Page's work. <sup>14</sup> Page included on Figure 20 data from AVCO <sup>29</sup>, <sup>33</sup>, his own work, and one free-flight result. <sup>34</sup> The free-flight result was not too well determined but was included to give a reference point at the higher velocity. Page considers the nonequilibrium radiative flux shown on the figure to be a reasonable upper limit and has shown the simulated altitude for each point on the figure. The figure then allows a comparison of values from different sources and shows that very similar results have been obtained, apparently within a factor of 2.

The above discussion has shown that the nonequilibrium radiative flux experienced by a vehicle during lunar return can probably be determined within a factor of two. Furthermore, it has been seen that the level of the nonequilibrium radiative flux is relatively very small when compared to other heating flux experienced by the Apollo CM (sometimes the order of 1000 watts/cm<sup>2</sup>). Hence, the present author feels that a drastic reinterpretation of the present data would have to occur before any nonequilibrium radiative flux changes would affect the heat shield design of the Apollo CM. That is, the most fruitful area in radiative heating deals with obtaining more precise tables for equilibrium  $E_T$  tables (including a detailed examination in the  $< .2\mu$  wavelength region), which should be settled before future effort is concerned with the nonequilibrium flux.



H. L. Davis

## BELLCOMM, INC.

### REFERENCES

1. A. H. Shapiro, "The Dynamics and Thermodynamics of Compressible Fluid Flow" (The Ronald Press Co., New York, 1953), Vol. I, p. 121.
2. P. V. Marrone, "Normal Shock Waves in Air: Equilibrium Composition and Flow Parameters for Velocities from 26,000 to 50,000 ft/sec," Cornell Aero. Lab. Report AG - 1729-A-2, August 1962.
3. C. F. Hansen, "Approximations for the Thermodynamic and Transport Properties of High Temperature Air," NASA TR R-50(1959).
4. J. Hilsenrath, M. Klein, and H. W. Woolley, "Tables of Thermodynamic Properties of Air Including Dissociation and Ionization from 1,500°K to 15,000°K," AEDC TR-59-20, December 1959.
5. W. E. Moeckel and K. C. Weston, "Composition and Thermodynamic Properties of Air in Chemical Equilibrium," NASA TN 4265(1958).
6. B. H. Wick, "Radiative Heating of Vehicles Entering the Earth's Atmosphere," AGARD Meeting on High Temperature Aspects of Hypersonic Flows, Brussels, Belgium, April 1962.
7. B. Kivel and K. Bailey, "Tables of Radiation from High Temperature Air," Res. Rept. 21, AVCO Res. Lab., December 1957.
8. P. H. Rose, "Radiation and Ionization Problems in Re-entry", Conference on Physics of the Solar System and Re-entry Dynamics, Langley Research Center, August 1961.
9. L. Lees, "Recovery Dynamics - Heat Transfer at Hypersonic Speeds in a Planetary Atmosphere," Space Technology edited by H. Seifert (John Wiley & Sons, Inc., New York, 1959).
10. R. E. Meyerott, J. Sokoloff, and R. A. Nicholls, "Absorption Coefficients of Air," Geophys. Res. Paper 68, AFCRC, Bedford, Mass., 1960.
11. P. D. Thomas, "Air Emissivity and Shock-Layer Radiation," J. Aerospace Sci. 29, 477(1962).

## BELLCOMM. INC.

12. B. Kivel, "Radiation from Hot Air and Stagnation Heating," Res. Rept. 79, AVCO Res. Lab., October 1959.
13. R. G. Breene, Maria Nardone, T. R. Riethof, and S. Zeldin, "Radiance of Species in High Temperature Air," GE R62SD52, General Electric Space Science Lab., July 1962.
14. W. A. Page, "Shock-Layer Radiation of Blunt Bodies Traveling at Lunar Return Entry Velocities," IAS Paper 63-41, January 1963.
15. Maria Nardone, R. G. Breene, S. Zeldin, and T. R. Riethof, "Radiance of Species in High Temperature Air," GE R63SD3, General Electric Space Sciences Lab., June 1963.
16. G. E. Kaattari, "Predicted Shock Envelopes About Two Types of Vehicles at Large Angles of Attack," NASA TN D - 860, April 1961.
17. J. G. Marvin, T. Tendeland, and M. Kussoy, "Apollo Forebody Pressure and Heat-Transfer Distributions in Helium at  $M_\infty = 20$ ," NASA TM X-854, November 1963 (CONFIDENTIAL).
18. H. de l'Estoile, and L. Rosenthal, "Rapid Evaluation of Radiant Heating During Re-entry into the Atmosphere," Aeronautics and Astronautics, Re-entry Proceedings of the Durant Centennial Conference, edited by N. J. Hoff and W. G. Vincenti (Pergamon Press, New York, 1960).
19. A. R. Hochstim, "Gas Properties Behind Shocks at Hypersonic Velocities. I. Normal Shocks in Air," Convair Rept. ZPh (GP)-002, January 1957.
20. G. E. Kaattari, "Predicted Gas Properties in the Shock Layer Ahead of Capsule-Type Vehicles at Angles of Attack," NASA TN D-1423, October 1962.
21. S. H. Maslen and W. E. Moeckel, "Inviscid Hypersonic Flow Past Blunt Bodies," Jour. Aero. Sci. 24, 683 (1957).
22. F. B. Fuller, "Numerical Solutions for Supersonic Flow of an Ideal Gas Around Blunt Two-Dimensional Bodies," NASA TN D-791, July 1961.
23. R. Goulard and M. Goulard, "One Dimensional Energy Transfer in Radiant Media," Int'l Jour. Heat and Mass Transfer 1, 81 (1960).

## BELLCOMM, INC.

24. R. Goulard, "A Comment on Radiation from Hot Air and Its Effect on Stagnation-Point Heating," Jour. Aerospace Sci. 28, 158 (1961).
25. H. Kennet and S. L. Strack, "Stagnation Point Radiative Transfer," ARS Jour. 31, 370. (1961).
26. S. L. Strack, "Radiant Heat Transfer Around Re-entry Bodies," ARS Jour. 32, 744 (1962).
27. K. K. Yoshikawa and D. R. Chapman, "Radiative Heat Transfer and Absorption Behind a Hypersonic Normal Shock Wave," NASA TN D - 1424, September 1962.
28. M. C. Adams, "A Look at the Heat Transfer Problem at Super Satellite Speeds," ARS Preprint 1556-60, December 1960.
29. J. D. Teare, S. Georgiev, and R. A. Allen, "Radiation from the Nonequilibrium Shock Front," Res. Rept. 112, AVCO Res. Labs., October 1961.
30. R. A. Allen, P. H. Rose, and J. C. Camm, "Nonequilibrium and Equilibrium Radiation at Super-Satellite Re-entry Velocities," Res. Rept. 156, AVCO Res. Labs., September 1962.
31. E. H. Kennard, Kinetic Theory of Gases (McGraw-Hill Book Co., Inc., 1938), p. 98.
32. S. Georgiev, J. D. Teare, and R. A. Allen, "Hypervelocity Radiative Heat Transfer," Res. Note 264, AVCO Res. Labs., August 1961.
33. J. C. Camm, B. Kivel, R. L. Taylor, and J. D. Teare, "Absolute Intensity of Nonequilibrium Radiation in Air and Stagnation Heating at High Altitudes," Res. Rept. 93, AVCO Res. Labs., December 1959.
34. T. N. Canning and W. A. Page, "Measurements of Radiation from the Flow Fields of Bodies Flying at Speeds up to 13.4 Kilometers per Second," Paper presented to AGARD, Brussels, Belgium, April 1962.
35. J. A. Fay and N. H. Kemp, "Theory of Stagnation-Point Heat Transfer in a Partially Ionized Diatomic Gas," AIAA Journal 1, 2741 (1963).

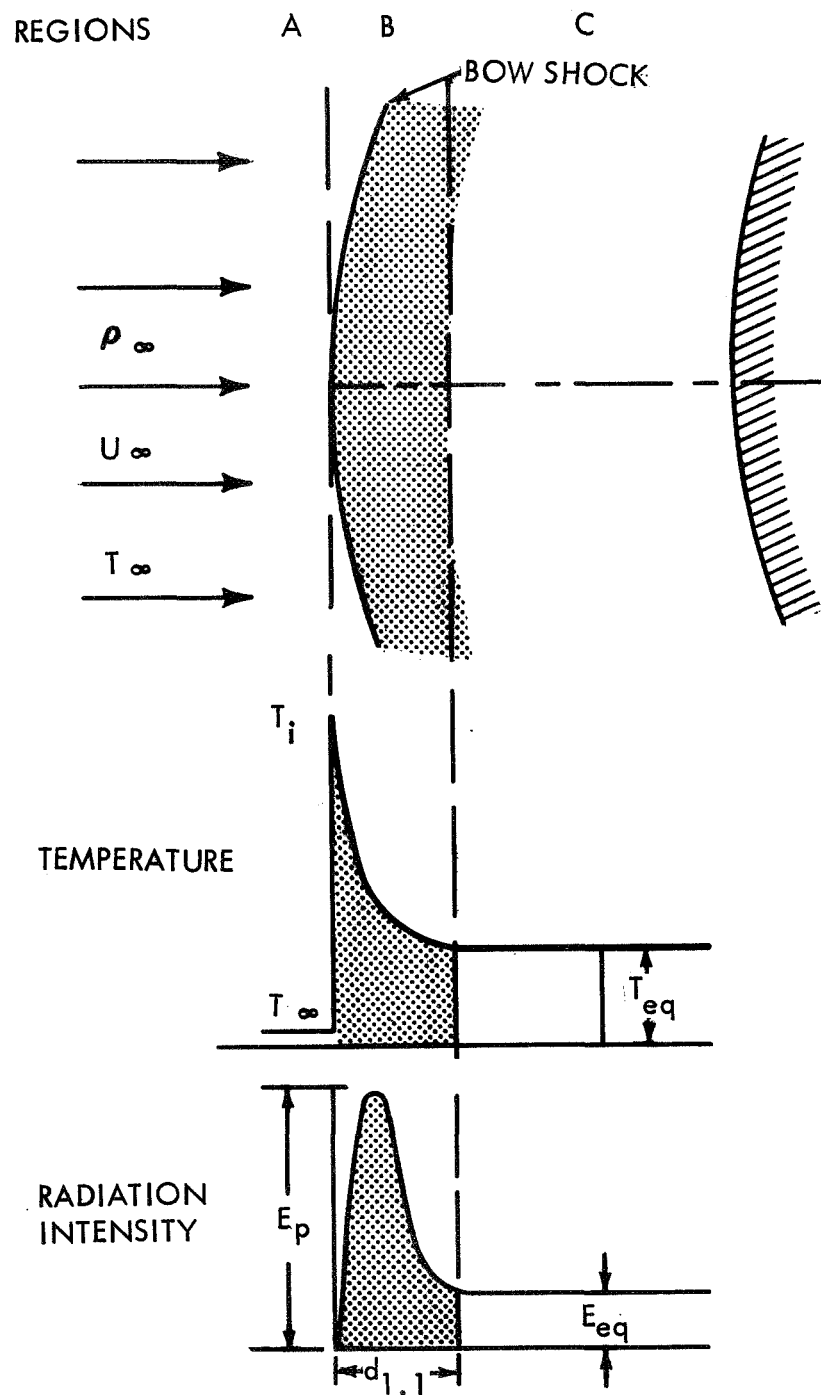


FIG. 1 SCHEMATIC DIAGRAM OF THE NON-EQUILIBRIUM REGION BEHIND THE BOW SHOCK AT THE STAGNATION POINT OF A BLUNT BODY.

(after Teare, Georgiev, & Allen, 1961)



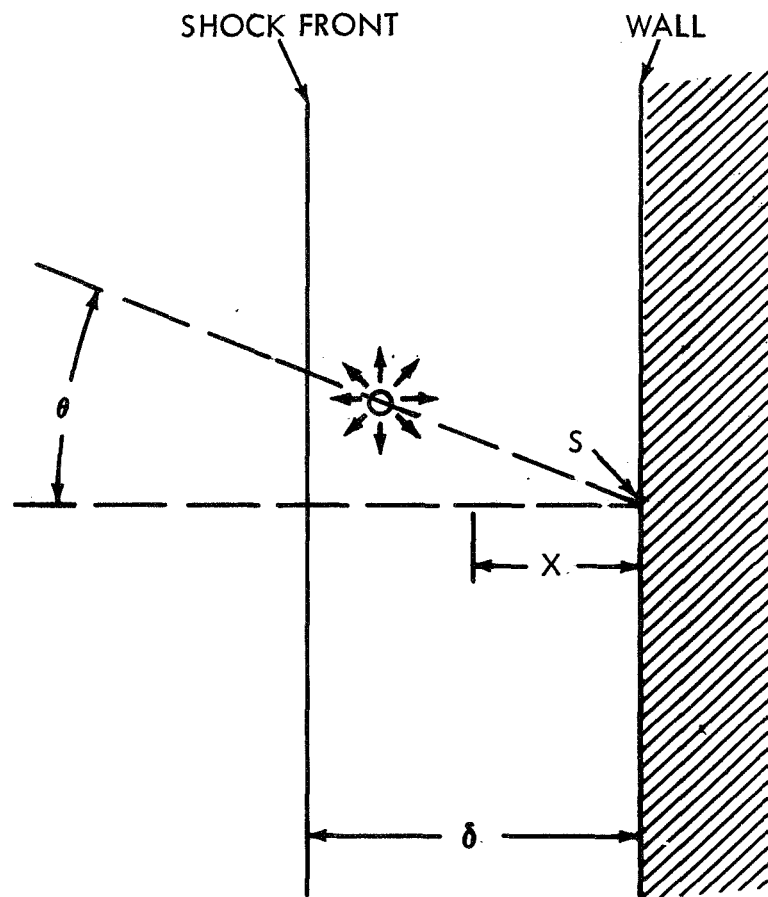


FIG. 2 PLANE LAYER APPROXIMATION FOR STAGNATION POINT HEATING.

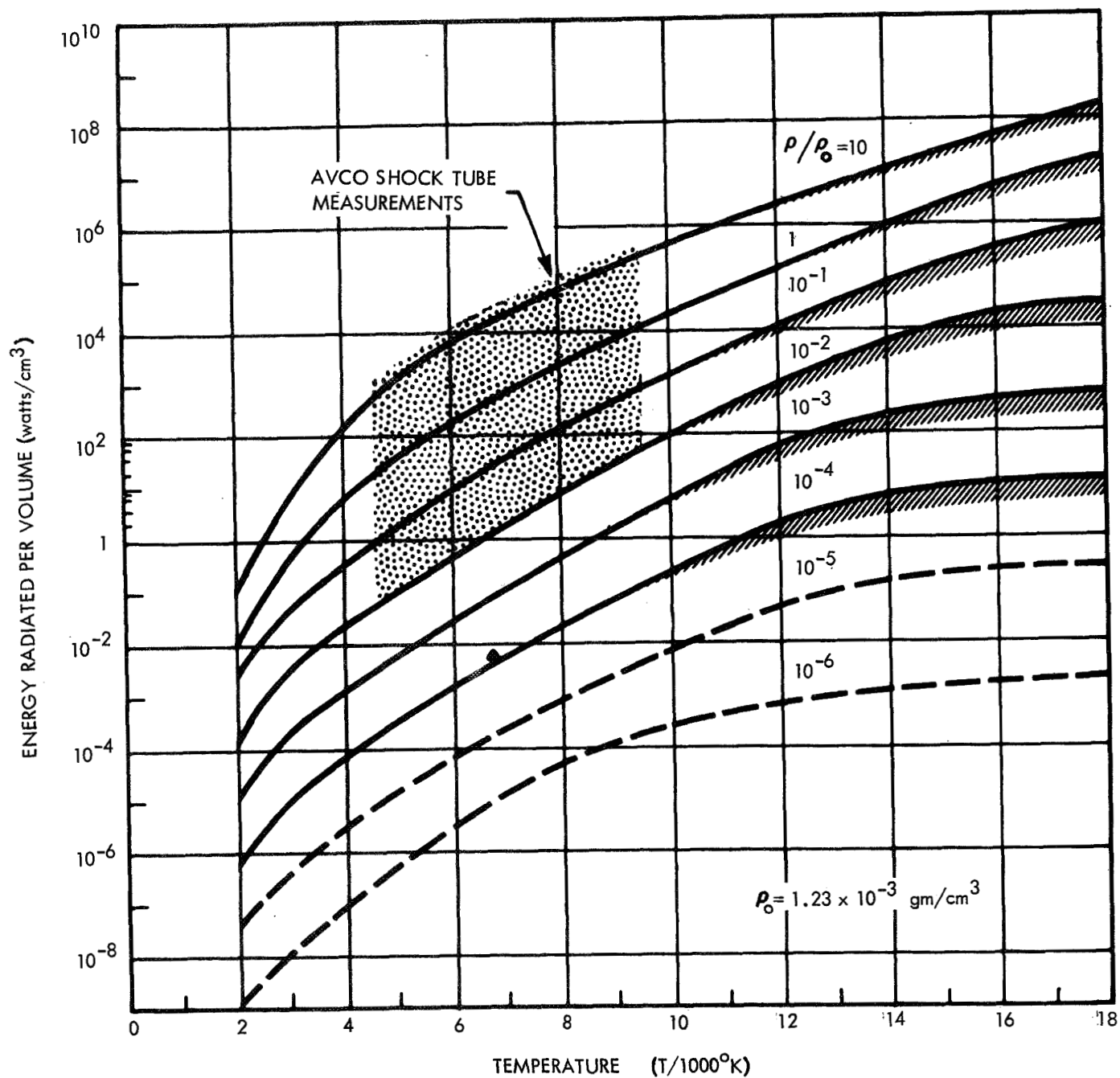


FIG. 3 TOTAL EMITTED RADIATION ENERGY PER UNIT VOLUME OF HIGH TEMPERATURE AIR IN FULL EQUILIBRIUM AS A FUNCTION OF TEMPERATURE FOR CONSTANT VALUES OF THE DENSITY.

(after Rose, 1961)

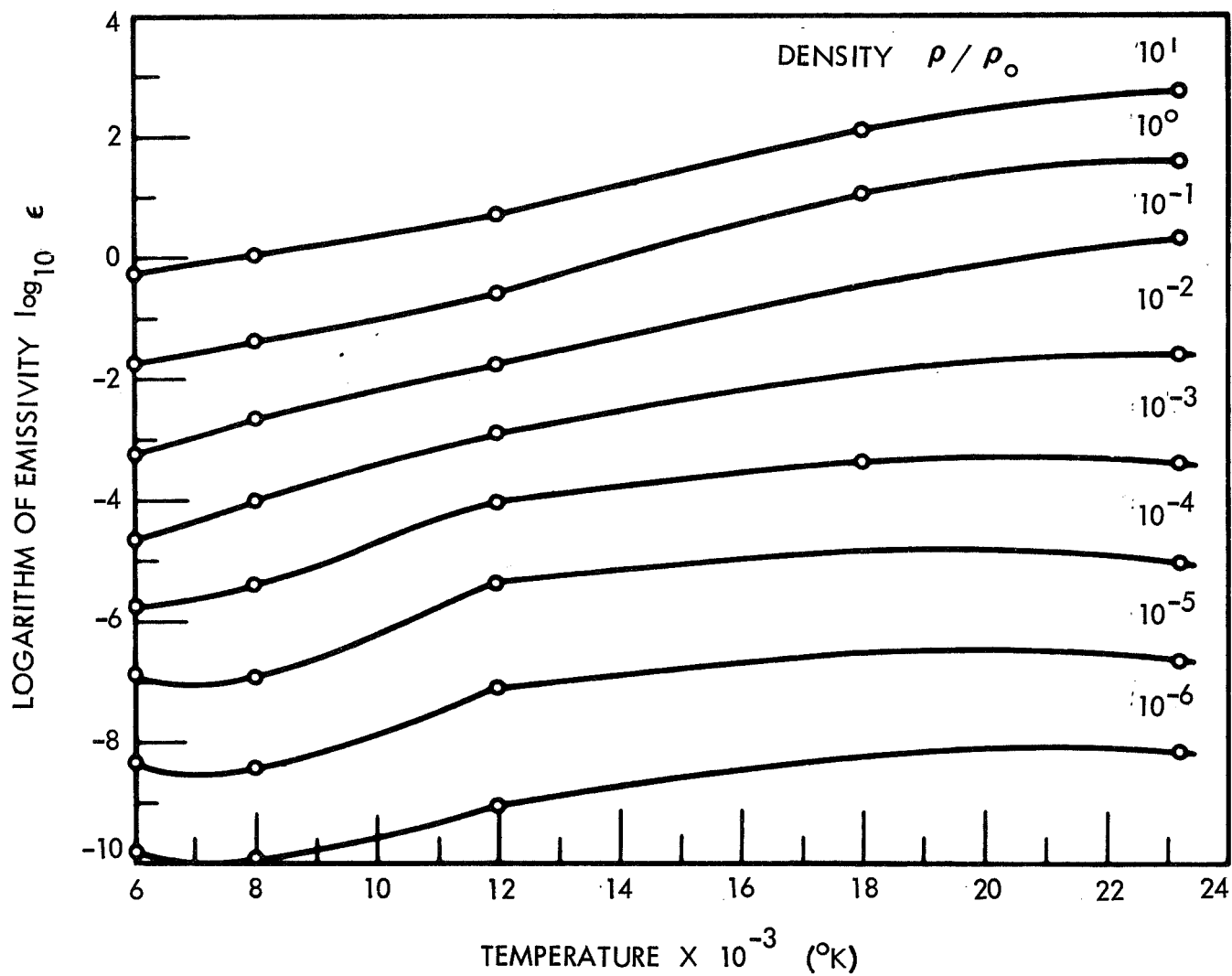


FIG. 4 EMISSIVITY OF HIGH TEMPERATURE AIR BASED ON WORK OF MEYEROTT, SOKOLOFF, AND NICHOLLS.

(after Thomas, 1962)

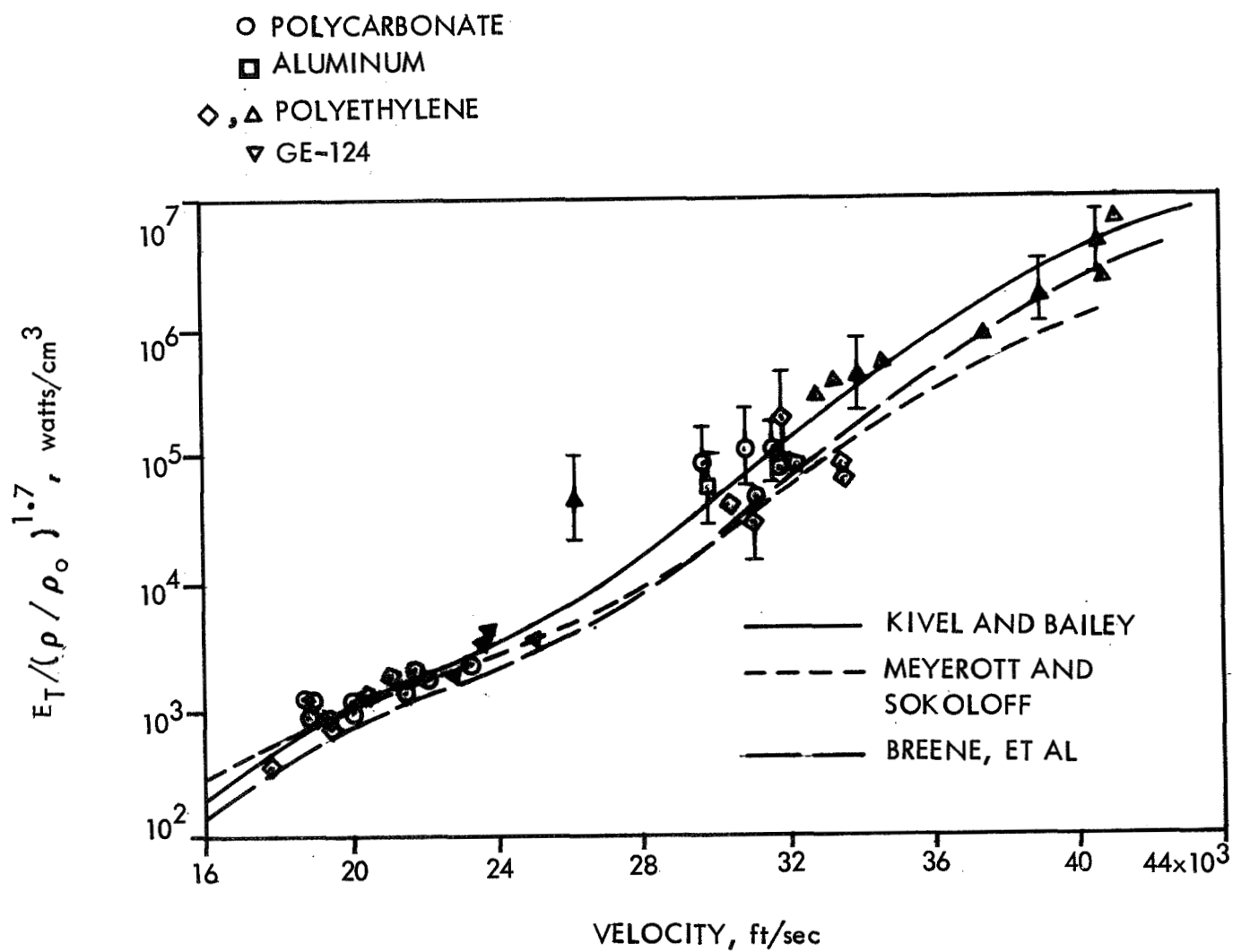


FIG. 5 EQUILIBRIUM AIR RADIATION, EXPERIMENT AND PREDICTIONS.

(after Page, 1963)

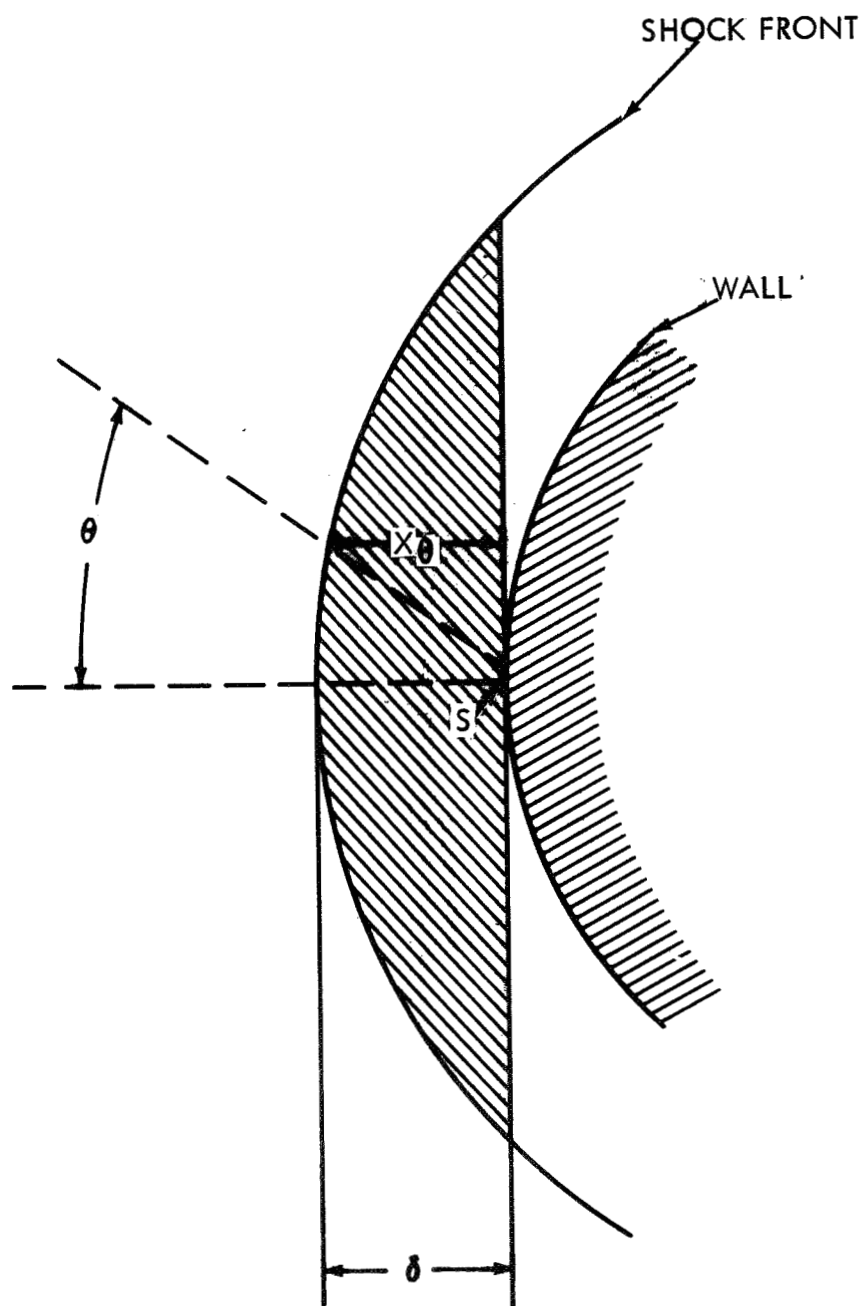


FIG. 6 STAGNATION POINT HEATING FOR A SPHERICAL SEGMENT SHOCK.

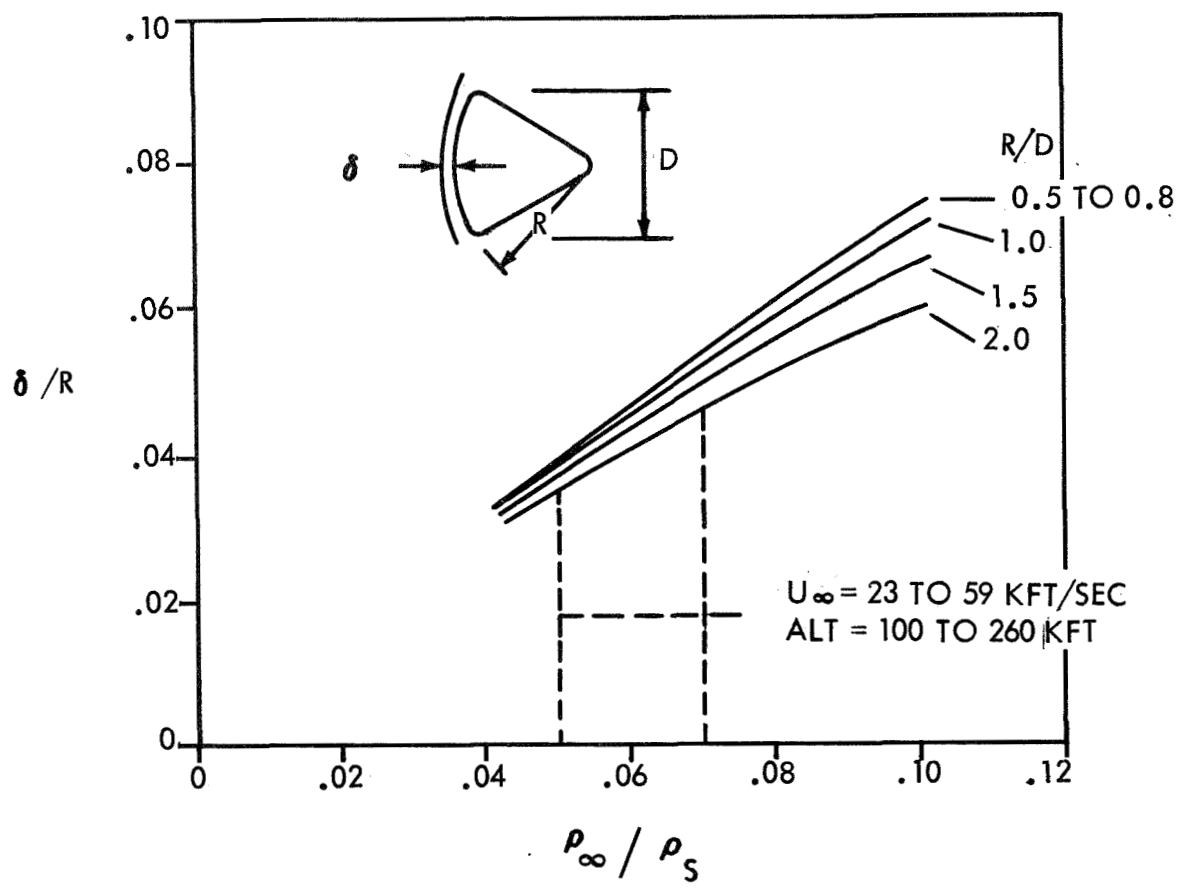
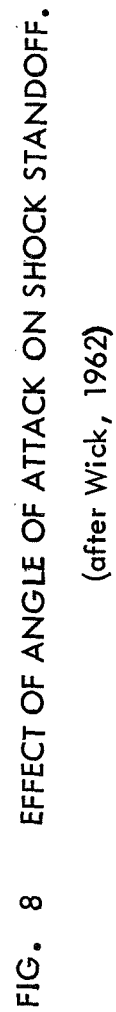


FIG. 7 - SHOCK STANDOFF FOR ZERO ANGLE OF ATTACK.

-(after Wick, 1962)



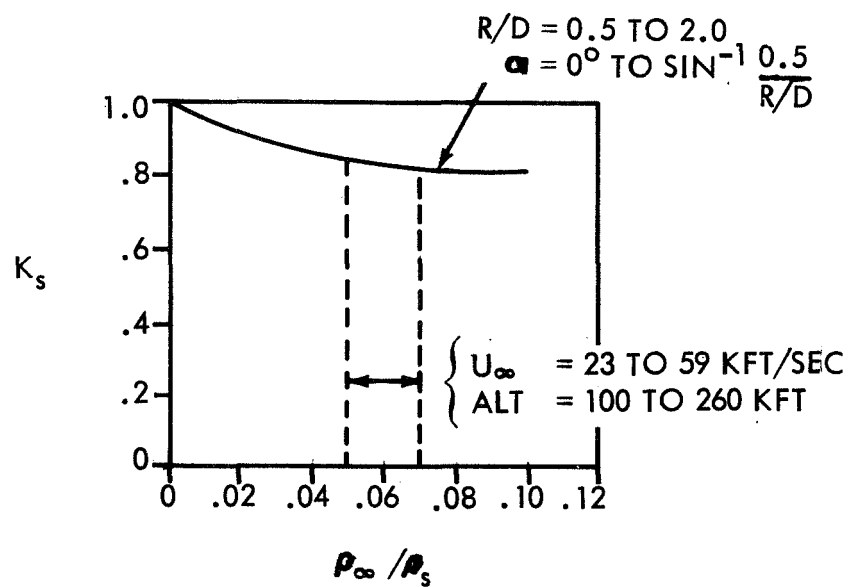


FIG. 9 SHOCK SHAPE FACTOR FOR STAGNATION POINT RADIATIVE FLUX.

(after Wick, 1962)



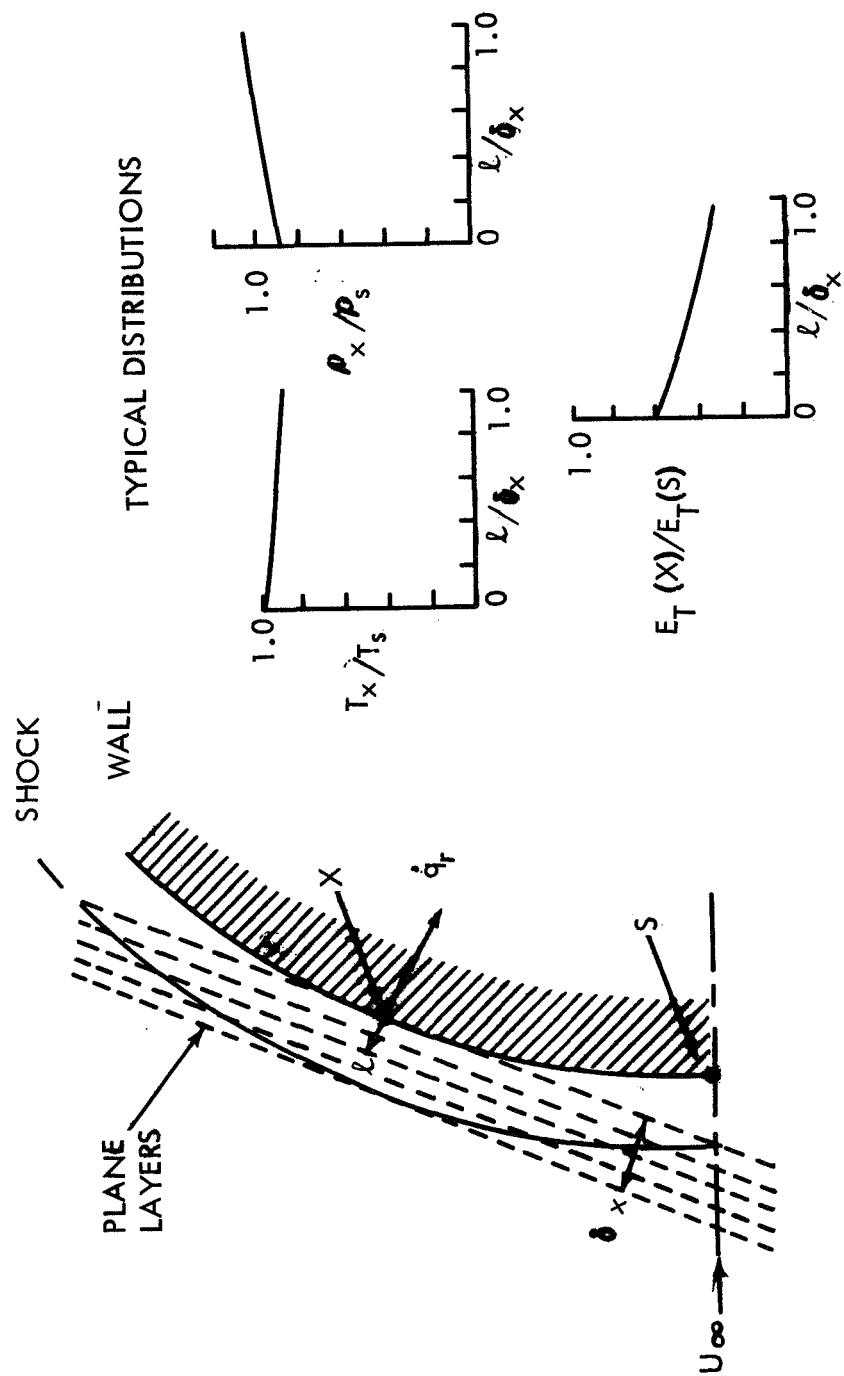


FIG. 10 ILLUSTRATION OF RADIATIVE FLUX DISTRIBUTION USING THE METHOD OF 'ESTOILE & ROSENTHAL.  
(after Wick, 1962)

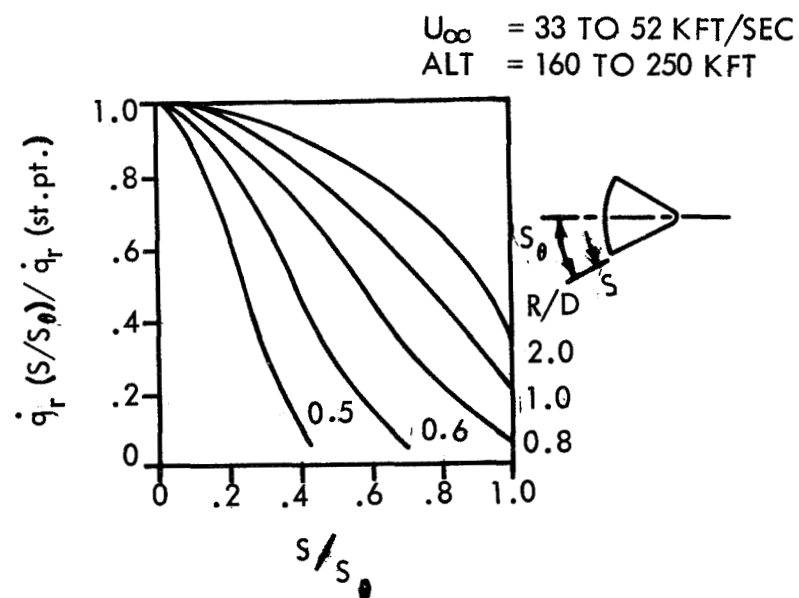


FIG. 11 RADIATIVE FLUX DISTRIBUTIONS AT ZERO ANGLE OF ATTACK.  
 (after Wick, 1962)

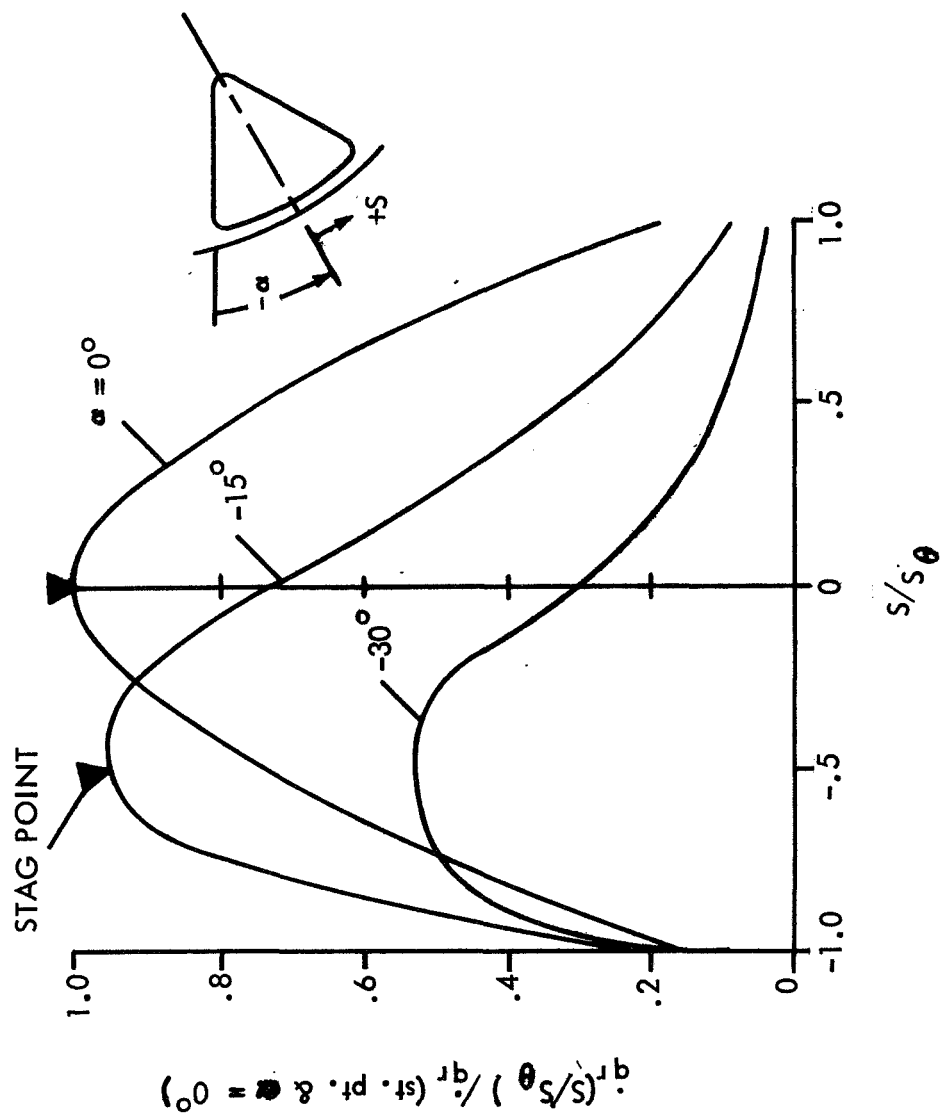
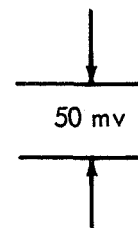
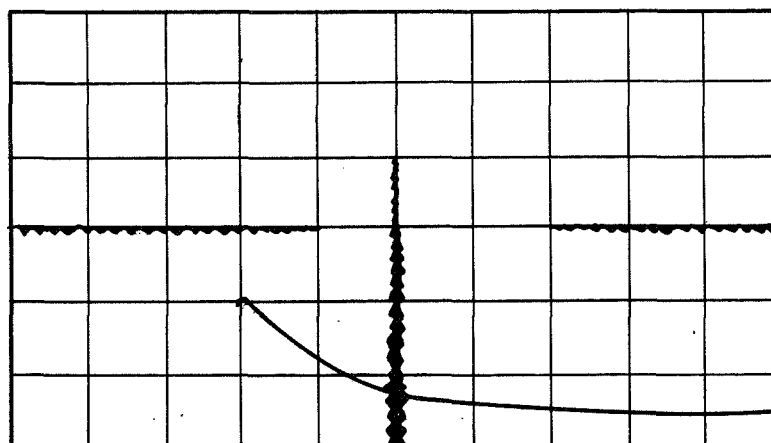


FIG. 12 - RADIATIVE FLUX DISTRIBUTIONS AT ANGLE OF ATTACK;  $R/D = 1.0$ .  
(after Wick, 1962)

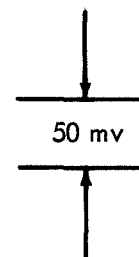
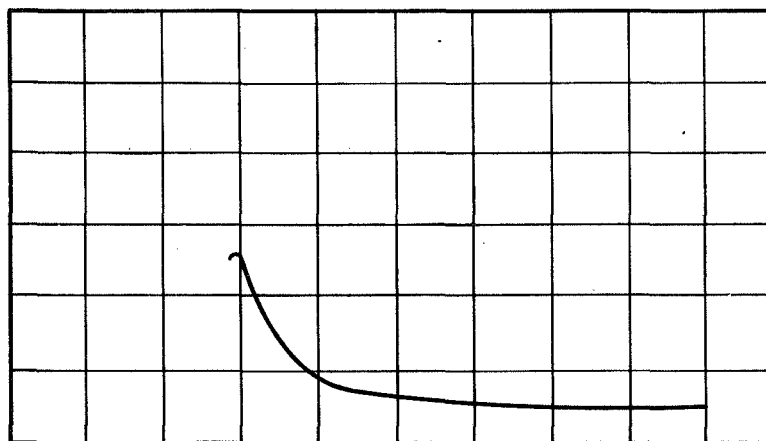
NITROGEN,  $P_1 = 2\text{ mm Hg}$ ,  $N_2(1+)$  RADIATION  $[.55 - 1.0 \mu]$

SHOCK VELOCITY

$5.18 \frac{\text{mm}}{\mu \text{ SEC}}$

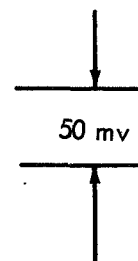
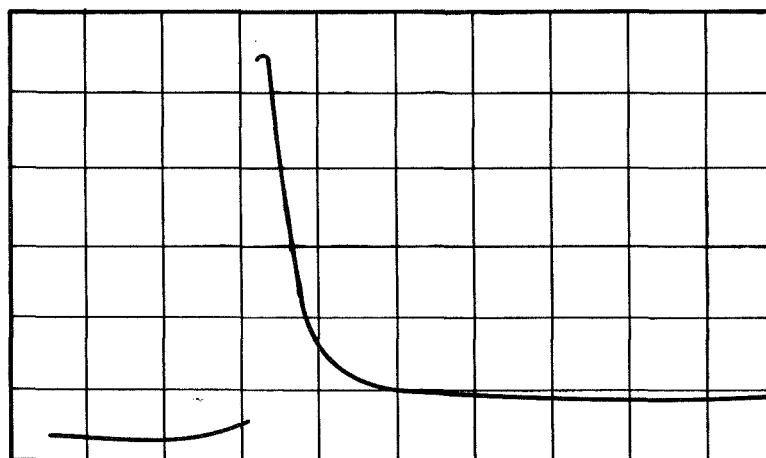


$5.54 \frac{\text{mm}}{\mu \text{ SEC}}$



↑  
INTENSITY

$6.08 \frac{\text{mm}}{\mu \text{ SEC}}$



← 1 μ sec

TIME →

FIG. 13 TYPICAL OSCILLOGRAMS OF THE  $N_2(1+)$  RADIATION FROM SHOCK WAVES IN PURE  $N_2$  SHOWING THE RADIATION OVERSHOOT BEHIND THE SHOCK FRONT AND SUBSEQUENT RELAXATION TO EQUILIBRIUM FOR SEVERAL SHOCK SPEEDS.

(after Rose, 1961)

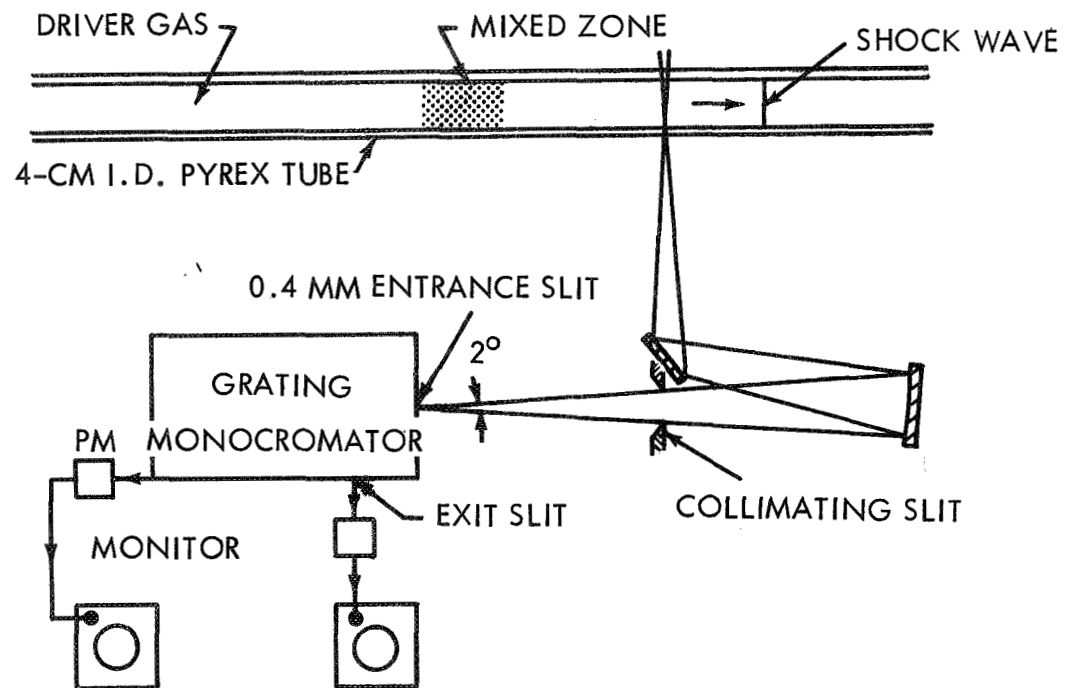


FIG. 14 SCHEMATIC DIAGRAM OF APPARATUS USED BY AVCO  
TO STUDY NONEQUILIBRIUM RADIATION

(after Rose, 1961)

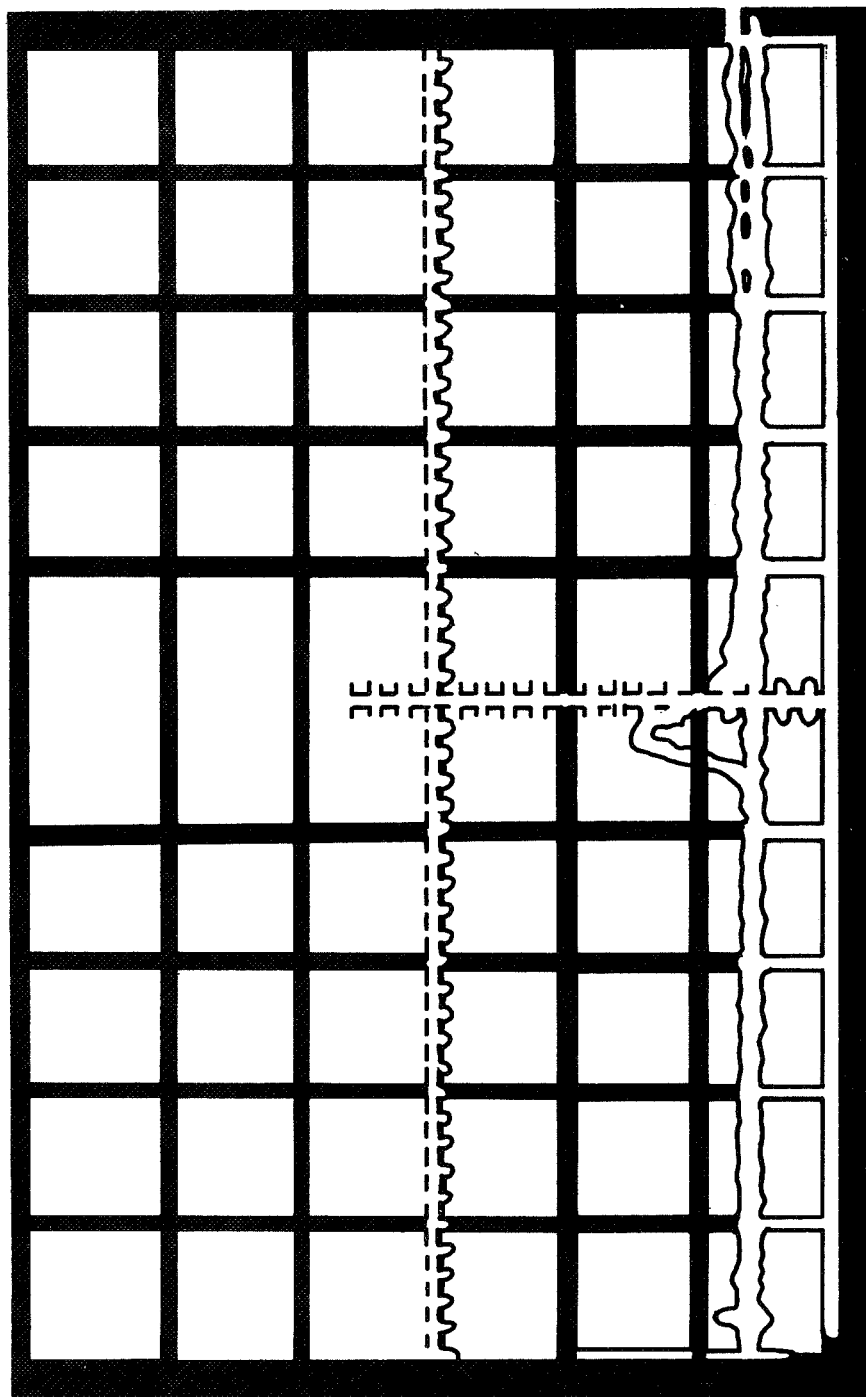
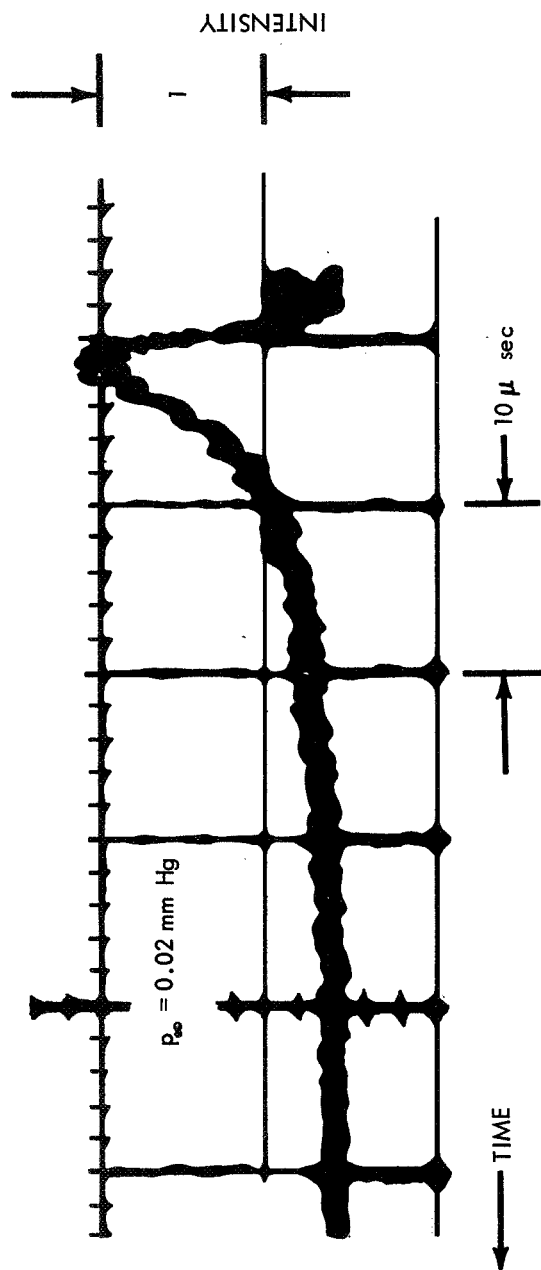
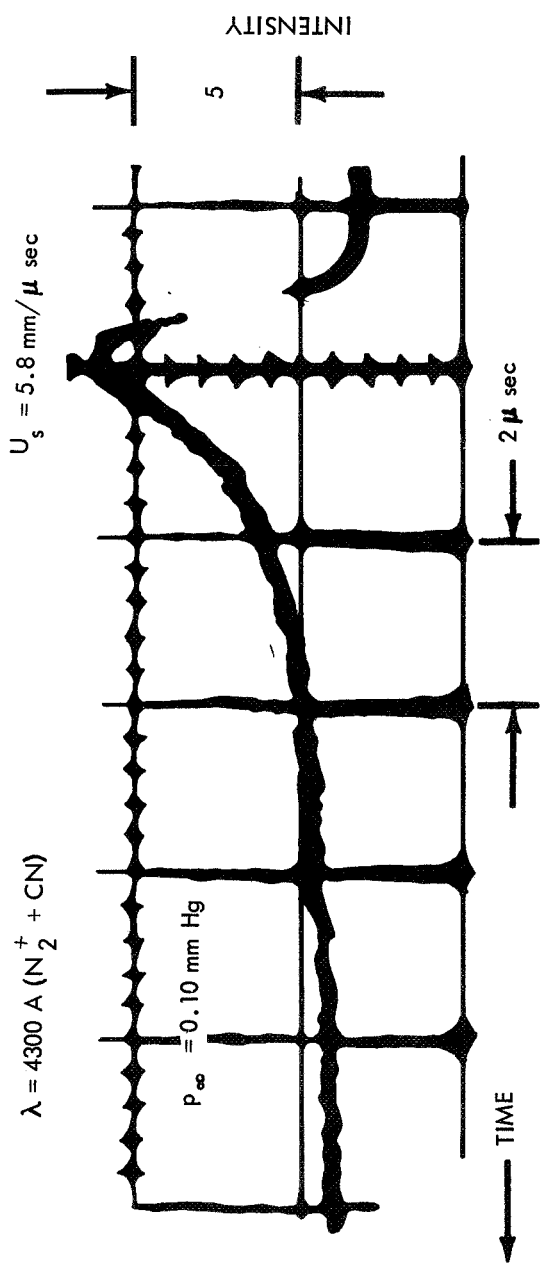


FIG. 15 OSCILLOGRAM OF THE NITROGEN FIRST POSITIVE RADIATION BEHIND A NORMAL SHOCK IN AIR IN AN ELECTRIC SHOCK TUBE. THE WAVELENGTH REGION IS 5000 Å - 10,000 Å.  $U_s = 33,000$  FT/SEC.  $P_\infty = 0.1$  mm Hg

(after Teare, Georgiev, & Allen, 1961)



RN 175

FIG. 16 TYPICAL RADIATION PROFILES BEHIND SHOCK WAVES IN AIR

(after Rose, 1961)

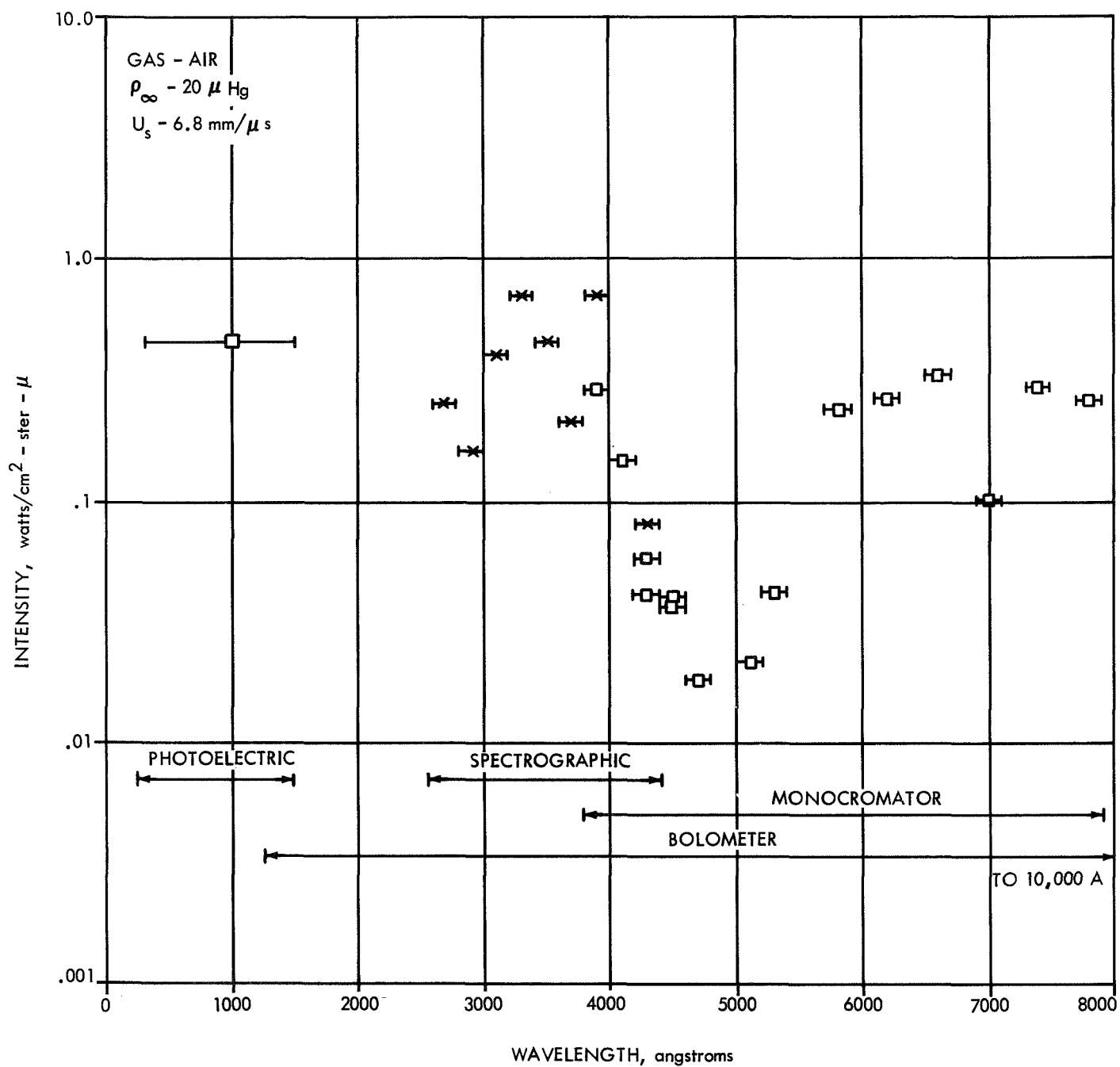


FIG. 17 MEASURED SPECTRAL INTENSITY OF A  $6.8 \text{ mm}/\mu \text{ s}$  SHOCK IN AIR AT A PRESSURE OF 20 MICRONS OF MERCURY.

(after Rose, 1961)



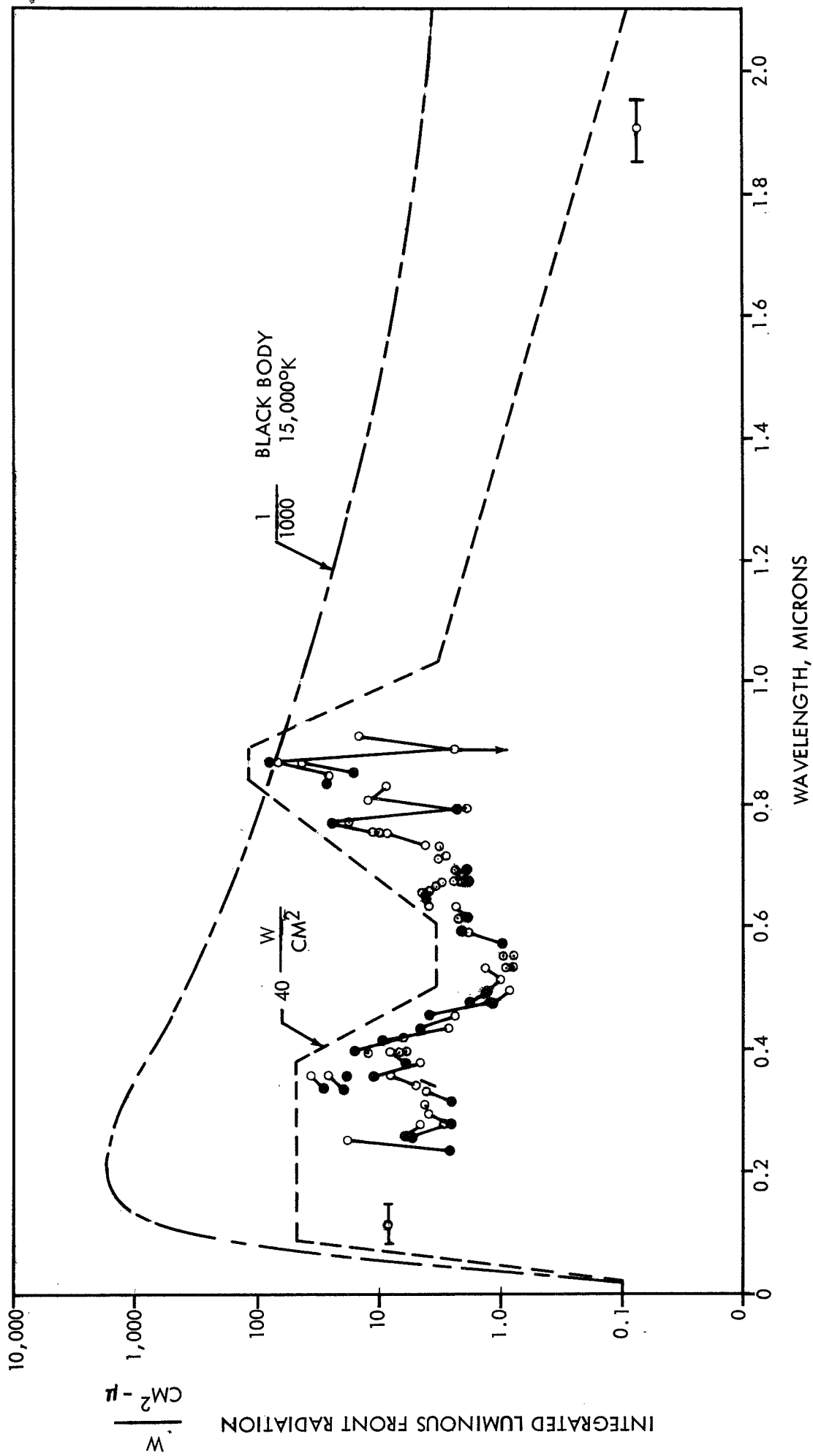
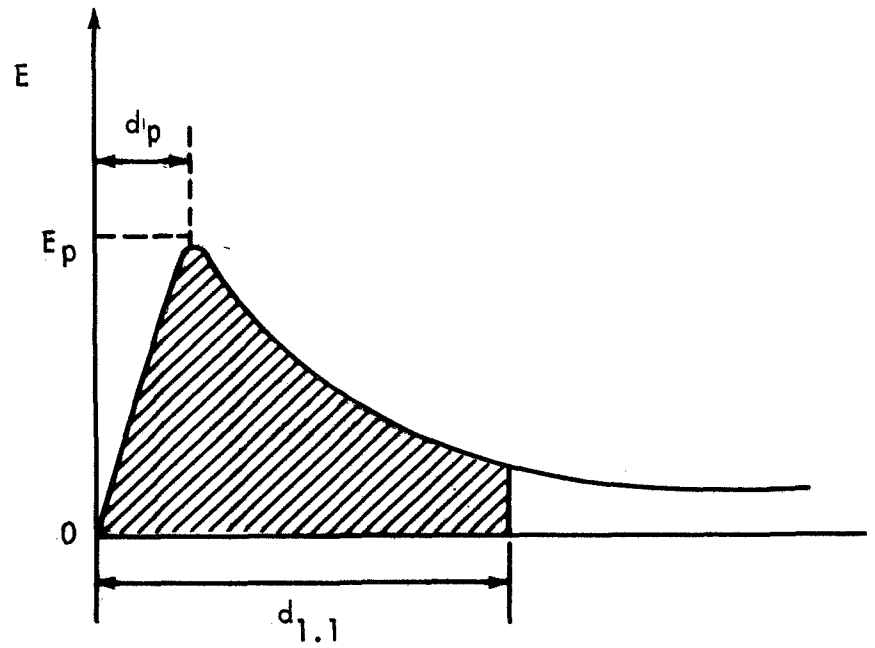


FIG. 18 NONEQUILIBRIUM RADIATION MEASUREMENTS OF NORMAL AIR SHOCKS VERSUS WAVELENGTH. THE SHOCK CONDITIONS ARE  $U_{\infty} = 10 \text{ mm}/\mu \text{ sec}$   $P_{\infty} = 0.1 \text{ mm Hg}$ . THE AREA UNDER THE DASHED CURVE IS  $40 \text{ watts/cm}^2 - .2 \pi \text{ ster}$ .

(After Allen, Rose, & Camm, 1962)



$$E_p \sim \rho$$

$$d_p \sim \rho^{-1}$$

$$d_{1.1} \sim \rho^{-1}$$

$$\text{Total} \sim E_p d_{1.1} \sim \text{const.}$$

FIG. 19 SCHEMATIC NONEQUILIBRIUM RADIATION PROFILE

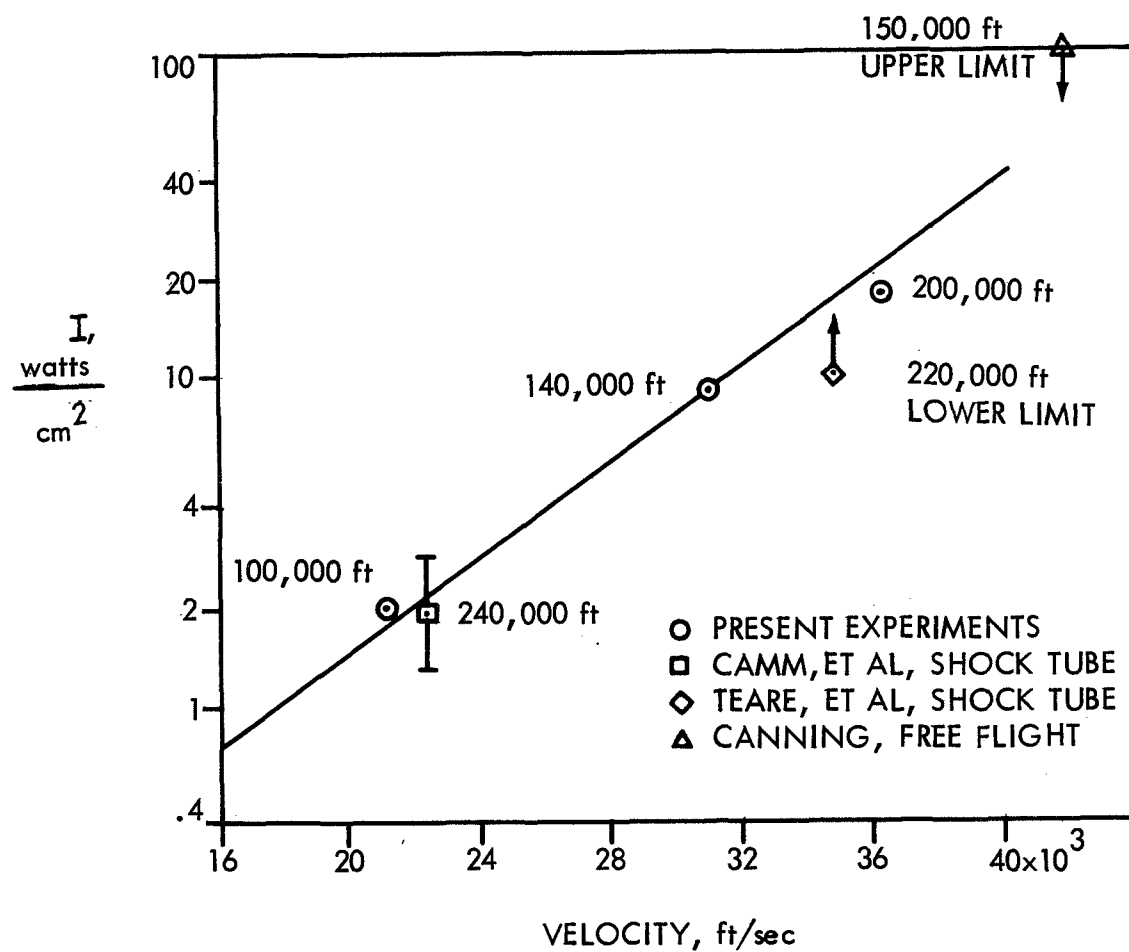


FIG. 20 SUMMARY OF AVAILABLE MEASUREMENTS OF NONEQUILIBRIUM AIR RADIATION.

(after Page, 1963)